Journal of Scientific Computing (2022) 92:96
https://doi.org/10.1007/s10915-022-01951-3

CVEM-BEM Coupling with Decoupled Orders for 2D Exterior Poisson Problems

Luca Desiderio[1] · **Silvia Falletta**[2] · **Matteo Ferrari**[2] · **Letizia Scuderi**[2]

Received: 15 December 2021 / Revised: 14 May 2022 / Accepted: 1 July 2022 /
Published online: 1 August 2022

Abstract
For the solution of 2D exterior Dirichlet Poisson problems, we propose the coupling of a Curved Virtual Element Method (CVEM) with a Boundary Element Method (BEM), by using decoupled approximation orders. We provide optimal convergence error estimates, in the energy and in the weaker L^2-norm, in which the CVEM and BEM contributions to the error are separated. This allows for taking advantage of the high order flexibility of the CVEM to retrieve an accurate discrete solution by using a low order BEM. The numerical results confirm the a priori estimates and show the effectiveness of the proposed approach.

Keywords Exterior Poisson problems · Curved virtual element method · Boundary element method · Coupling · Error estimates

Mathematics Subject Classification 35A01 · 65L10 · 65L12 · 65L20 · 65L70

L. Desiderio, S. Falletta, M. Ferrari, L. Scuderi: These authors contributed equally to this work.

✉ Silvia Falletta
silvia.falletta@polito.it

Luca Desiderio
luca.desiderio@unipr.it

Matteo Ferrari
matteo.ferrari@polito.it

Letizia Scuderi
letizia.scuderi@polito.it

[1] Dipartimento di Scienze Matematiche, Fisiche e Informatiche, Università di Parma, Parco Area delle Scienze, 7/A, Parma 43124, Italy

[2] Dipartimento di Scienze Matematiche "G.L. Lagrange", Politecnico di Torino, Corso Duca degli Abruzzi, 24, Torino 10129, Italy

1 Introduction

In this paper we deal with the following 2D problem

$$\begin{cases} -\Delta u_e(\mathbf{x}) = f(\mathbf{x}) & \mathbf{x} \in \Omega_e, \\ u_e(\mathbf{x}) = 0 & \mathbf{x} \in \Gamma_0, \end{cases} \tag{1}$$

where $\Omega_e := \mathbf{R}^2 \setminus \overline{\Omega}_0$ is an unbounded domain, exterior to an open bounded one Ω_0, with Lipschitz boundary Γ_0. It is known (see [1] and the references therein) that Problem (1) admits a unique solution in the space

$$W^1(\Omega_e) := \left\{ v : \omega v \in L^2(\Omega_e), \nabla v \in [L^2(\Omega_e)]^2 \right\}$$

with $\omega(\mathbf{x}) := \left(\sqrt{1+\|\mathbf{x}\|^2}\left(1+\log\left(\sqrt{1+\|\mathbf{x}\|^2}\right)\right)\right)^{-1}$, satisfying the asymptotic conditions

$$u_e(\mathbf{x}) = \alpha + O\left(\frac{1}{\|\mathbf{x}\|}\right) \quad \text{and} \quad \nabla u_e(\mathbf{x}) = O\left(\frac{1}{\|\mathbf{x}\|^2}\right) \quad \text{for} \quad \|\mathbf{x}\| \to \infty. \tag{2}$$

The constant α represents the asymptotic behaviour of u_e at infinity and, here, its value is not fixed in advance.

The above problem is of interest in many engineering and physical applications, for example when studying electric and thermal plane fields on infinite domains produced by point sources, or when solving problems of fluid flows around obstacles. Many and various numerical methods have been proposed and analysed for its solution, among which we mention the traditional Boundary Element Method (BEM). This latter is the most natural way to deal with unbounded domains (for a reference, see [2] and the bibliography therein contained). Another common approach is the coupling of a classical variational or finite difference method with a transparent (absorbing or non-reflecting) condition defined on an artificial boundary Γ, properly chosen to delimit a finite computational domain. Among the most commonly used Non-Reflecting Boundary Conditions (NRBCs), those of integral type are exact (i.e. not approximated) and allow for treating artificial boundaries of arbitrary, even non-convex, shapes.

The aim of this paper is to propose such a coupling by means of the interior Curved Virtual Element Method (CVEM) and the one-equation BEM. Standard VEMs have been applied to a wide variety of interior problems (see the pioneering [3] for the Poisson problem and [4–7] for more recent applications), but only few papers deal with exterior problems (see [8–11] for elliptic equations). Among the CVEM approaches till now investigated, we mention those proposed in [12] and [13]. Although the latter deals with local polynomial preserving VEM spaces, we focus on the former since it is well-suited for problems characterized by computational domains with prescribed curved boundaries, like ours.

The choice of using VEM, or the more general CVEM, is mainly motivated by the following reasons: it allows us to consider meshes whose elements can be of general shape, and to define local discrete spaces in such a way that the elementary stiffness matrix can be computed using only the degrees of freedom, without the need of explicitly knowing the expression of the non-polynomial functions (whence the "virtual" word comes). Hence, arbitrarily high order VEM can be easily applied by maintaining the simplicity of the implementation. Moreover, the nature of the VEM allows for decoupling the approximation orders and the mesh grids associated with the domain and boundary methods, without the need of using special auxiliary variables (like mortar ones) for the coupling. Indeed, by exploiting the peculiar construction of the VEM, it is possible to add hanging nodes on the edges of the

elements that belong to the artificial boundary, without significantly modifying the structure of the interior mesh.

It is worth pointing out that the definition of the discrete VEM spaces has the same implicit nature of that used by the Boundary Element-Based Finite Element Methods (BEM-based FEMs) (see, for example, [14]) and by the Trefftz-type Finite Element Methods (Trefftz-FEMs) (see, for example, [15] and the more recent [16] where curved elements have been considered). The main difference between BEM-based FEMs or Trefftz-FEMs and VEMs consists in the construction of the matrices involved in the final linear system. Indeed, contrary to VEMs, the computation of the matrix entries by the above mentioned methods is performed by point-wise evaluations of the basis functions and some of their derivatives in the interior of the mesh elements. Such basis functions are defined implicitly in terms of Poisson problems, with explicitly given polynomial data, and their values at the required points are computed first by solving the associated local Boundary Integral Equations (BIEs), and then by using the corresponding boundary integral representations. Moreover, we recall that, in the FEM context, various strategies have been proposed to deal with curved edges (see [17] for a survey), among which we mention the isoparametric FEM, in which the elements are mapped with high order polynomial maps that allow for a better approximation of the domain of interest. The advantage of VEMs with respect to isoparametric FEMs is that no approximation of the domain (even by polynomial functions) is introduced and no *ad hoc* positioning of the isoparametric nodes is needed. Furthermore, to the best of our knowledge, besides the curved versions of VEMs, in literature there are few methods which are able to make use of polytopal meshes with curvilinear edges, e.g. [18–20]. However, as far as the internal degrees of freedom are concerned, on triangles or quadrilaterals, VEMs are more expensive than the traditional FEMs.

For what concerns the one-equation BEM, we recall that it has been proposed in the well known Johnson & Nédélec Coupling (JNC) (see [1, 21]) and it is based on a single BIE that involves the integral operators associated with the fundamental solution (and its normal derivative) of the Laplace equation.

In the recent work [8], in which a similar problem has been studied, the authors consider the Costabel & Han Coupling (CHC) (see [22, 23]) combined with an interior VEM. This approach yields to a symmetric and non-positive definite scheme but, involving a BIE of hypersingular type, turns out to be quite onerous from the computational point of view. Even if the CHC has been applied in several contexts, the JNC turns out to be very appealing from the engineering point of view, this latter being cheaper and easier to implement. We remark in addition that, unlikely in [8], here we deal with the asymptotic condition (2) that entails

$$\int_{\Gamma} \lambda_e(\mathbf{y}) \mathrm{d}\Gamma_{\mathbf{y}} = 0, \tag{3}$$

where $\lambda_e(\mathbf{y}) := \frac{\partial u_e}{\partial \mathbf{n}}(\mathbf{y})$ denotes the normal derivative of u_e along the artificial boundary Γ. As a consequence, suitable spaces satisfying identity (3) have to be considered.

For the discretization of our coupled problem we consider a full Galerkin approach based on a CVEM in the interior of the computational domain and on a BEM associated with basis functions chosen in such a way that (3) is satisfied. We study the proposed approach from the theoretical point of view in a quite general framework, and we provide optimal error estimates in the energy and in the weaker L^2-norm. In particular, since we consider here curved domains, the use of curvilinear elements instead of polygonal ones, allows us to reach the optimal convergence rate for degrees of accuracy higher than 2, avoiding the sub-optimal rate caused by the approximation of the domain.

By a careful study, we show that the source of the approximation error of the discrete solution, both in the energy and in the L^2-norm, can be split into two contributions: a boundary (BEM) and an interior (CVEM) one. In particular, we show that the boundary contribution behaves like $h_\partial^{k_\partial}$ (h_∂ denoting the maximum edge length of the artificial boundary and k_∂ representing the BEM polynomial degree of accuracy), and the interior one like $h_\circ^{k_\circ}$ ($h_\circ$ being the maximum of the element diameters and $k_\circ$ the CVEM order degree). Hence, for $h_\partial \ll h_\circ$ and by fixing k_∂, it results that the bulk error dominates the boundary one up to a certain CVEM order, an aspect that allows us to reach a high accuracy of the global scheme with a low BEM order.

The paper is organized as follows: in the next section we present the model problem for the Poisson equation and its reformulation in a bounded region, obtained by introducing the artificial boundary and its associated one equation Boundary Integral NRBC (BI-NRBC). In Sect. 3 we introduce the variational formulation of the problem restricted to the finite computational domain. In Sect. 4 we apply the Galerkin method and we prove error estimates in the energy and in the L^2-norm in an abstract framework, provided that suitable hypotheses are assumed. Then we show that these latter are satisfied by the CVEM-BEM approximation spaces introduced in Sect. 5. Finally, in the last section we detail the choice of the particular basis functions used for the approximation of the normal derivative unknown, and we present some numerical test which confirm the theoretical results.

2 The Model Problem

Let $\Omega_e := \mathbf{R}^2 \setminus \overline{\Omega}_0$ be an unbounded domain, exterior to an open bounded domain $\Omega_0 \subset \mathbf{R}^2$, and denote by $\Gamma_0 := \partial\Omega_e$ its Lipschitz boundary having positive Haussdorf measure (see Fig. 1 (a)). We consider the exterior Dirichlet Poisson problem (1) in the unknown solution u_e, where $f \in L^2(\Omega_e)$ represents a source term having a compact support in Ω_e.

To determine the solution u_e of Problem (1) by means of an interior domain method, we surround the physical obstacle Ω_0 by an artificial boundary Γ; this allows for decomposing Ω_e into a finite computational domain Ω, bounded internally by Γ_0 and externally by Γ, and an infinite residual one, denoted by Ω_∞ (see Fig. 1 (b)). For the theoretical analysis of the numerical approach we propose, we need to assume that Γ_0 consists of a finite number of curves of class C^{m+1}, with $m \geq 0$, and that Γ is a contour of class C^∞.
Denoting by u and u_∞ the restrictions of the solution u_e to Ω and Ω_∞ respectively, and by $\mathbf{n}$ and $\mathbf{n}_\infty$ the unit normal vectors on Γ pointing outside Ω and Ω_∞ (consequently $\mathbf{n}_\infty = -\mathbf{n}$), we consider the following compatibility and equilibrium conditions on Γ:

$$u(\mathbf{x}) = u_\infty(\mathbf{x}), \qquad \frac{\partial u}{\partial \mathbf{n}}(\mathbf{x}) = -\frac{\partial u_\infty}{\partial \mathbf{n}_\infty}(\mathbf{x}), \qquad \mathbf{x} \in \Gamma. \tag{4}$$

In the above relations and in the sequel we omit, for simplicity, the use of the trace operators to indicate the restriction of H^1 functions to the boundary Γ from the exterior or interior.

Assuming, for simplicity, that Γ is chosen such that $\mathrm{supp}(f)$ is a bounded subset of Ω, the following Kirchhoff's formula

$$u_\infty(\mathbf{x}) = \int_\Gamma G(\mathbf{x}, \mathbf{y}) \frac{\partial u_\infty}{\partial \mathbf{n}_\infty}(\mathbf{y})\, \mathrm{d}\Gamma_\mathbf{y} - \int_\Gamma \frac{\partial G}{\partial \mathbf{n}_{\infty,\mathbf{y}}}(\mathbf{x}, \mathbf{y}) u_\infty(\mathbf{y})\, \mathrm{d}\Gamma_\mathbf{y} + \alpha, \quad \mathbf{x} \in \Omega_\infty \setminus \Gamma, \tag{5}$$

allows us to represent the solution u_∞ in Ω_∞. In (5), G and $\partial G/\partial \mathbf{n}_{\infty,\mathbf{y}}$ denote, respectively, the fundamental solution of the 2D Laplace equation and its normal derivative with respect

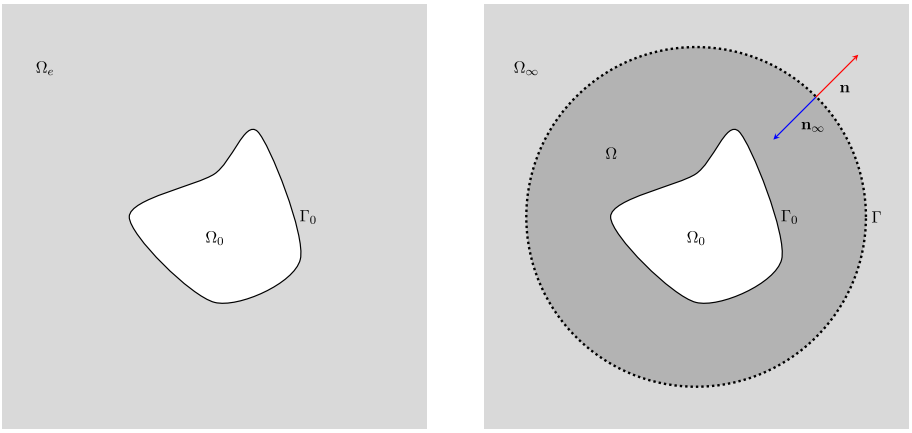

(a) **(b)**

Fig. 1 Model problem setting

to the unit vector $\mathbf{n}_{\infty,\mathbf{y}}$ having initial point in $\mathbf{y} \in \Gamma$. Their expression is given by

$$G(\mathbf{x},\mathbf{y}) = -\frac{1}{2\pi}\log r \quad \text{and} \quad \frac{\partial G}{\partial \mathbf{n}_{\infty,\mathbf{y}}}(\mathbf{x},\mathbf{y}) = \frac{1}{2\pi}\frac{\mathbf{r}\cdot\mathbf{n}_{\infty,\mathbf{y}}}{r^2},$$

where $r = \|\mathbf{r}\| = \|\mathbf{x}-\mathbf{y}\|$. It is known that the trace of (5) on Γ reads

$$\frac{1}{2}u_\infty(\mathbf{x}) - \mathrm{V}\frac{\partial u_\infty}{\partial \mathbf{n}_\infty}(\mathbf{x}) - \mathrm{K}u_\infty(\mathbf{x}) - \alpha = 0, \qquad \mathbf{x}\in\Gamma, \tag{6}$$

where $\mathrm{V}\colon H^{-1/2}(\Gamma) \to H^{1/2}(\Gamma)$ and $\mathrm{K}\colon H^{1/2}(\Gamma) \to H^{1/2}(\Gamma)$ represent, respectively, the continuous (see [24]) single- and double-layer integral operators, defined by

$$\mathrm{V}\psi(\mathbf{x}) := \int_\Gamma G(\mathbf{x},\mathbf{y})\psi(\mathbf{y})\,\mathrm{d}\Gamma_\mathbf{y}, \qquad \mathbf{x}\in\Gamma$$

and

$$\mathrm{K}\varphi(\mathbf{x}) := -\int_\Gamma \frac{\partial G}{\partial \mathbf{n}_{\infty,\mathbf{y}}}(\mathbf{x},\mathbf{y})\varphi(\mathbf{y})\,\mathrm{d}\Gamma_\mathbf{y}, \qquad \mathbf{x}\in\Gamma.$$

To determine the solution of Problem (1) in the finite computational domain Ω, we impose (6) as BI-NRBC on Γ. In particular, introducing the additional unknown $\lambda(\mathbf{y}) := \dfrac{\partial u}{\partial \mathbf{n}}(\mathbf{y})$ and taking into account (4), the new problem defined in Ω takes the form:

$$\begin{cases} -\Delta u(\mathbf{x}) = f(\mathbf{x}) & \mathbf{x}\in\Omega, \quad (7a)\\ u(\mathbf{x}) = 0 & \mathbf{x}\in\Gamma_0, \quad (7b)\\ \dfrac{1}{2}u(\mathbf{x}) + \mathrm{V}\lambda(\mathbf{x}) - \mathrm{K}u(\mathbf{x}) - \alpha = 0 & \mathbf{x}\in\Gamma. \quad (7c) \end{cases}$$

We point out that the asymptotic conditions (2) coupled with (7c) imply that $\langle\lambda, 1\rangle_\Gamma = 0$, where $\langle\cdot,\cdot\rangle_\Gamma$ denotes the duality pairing between $H^{-1/2}(\Gamma)$ and $H^{1/2}(\Gamma)$. This justifies the introduction of the space

$$H_0^{-1/2}(\Gamma) := \left\{ \lambda \in H^{-1/2}(\Gamma) \ : \ \langle \lambda, 1 \rangle_\Gamma = 0 \right\}$$

in which we will look for the unknown λ.

3 The Variational Formulation

Let us introduce the bilinear form $a : H^1(\Omega) \times H^1(\Omega) \to \mathbf{R}$

$$a(u, v) := \int_\Omega \nabla u(\mathbf{x}) \cdot \nabla v(\mathbf{x}) \, \mathrm{d}\mathbf{x}.$$

The variational formulation of Problem (7) consists in finding $u \in H^1_{0,\Gamma_0}(\Omega) := \{u \in H^1(\Omega) : u = 0 \text{ on } \Gamma_0\}$ and $\lambda \in H_0^{-1/2}(\Gamma)$ such that

$$\begin{cases} a(u, v) - \langle \lambda, v \rangle_\Gamma = (f, v)_{L^2(\Omega)} & \forall\, v \in H^1_{0,\Gamma_0}(\Omega), \qquad (8a) \\ \langle \mu, \left(\frac{1}{2} \mathrm{I} - \mathrm{K} \right) u \rangle_\Gamma + \langle \mu, \mathrm{V}\lambda \rangle_\Gamma = 0 & \forall\, \mu \in H_0^{-1/2}(\Gamma), \qquad (8b) \end{cases}$$

where I stands for the identity operator and $(\cdot, \cdot)_{L^2(\Omega)}$ denotes the $L^2(\Omega)$-inner product. It is worth noting that, since we test Equation (7c) with $\mu \in H_0^{-1/2}(\Gamma)$, satisfying by definition $\langle \mu, 1 \rangle_\Gamma = 0$, the unknown constant α does not appear in the variational formulation (8). Nevertheless, the asymptotic behaviour α is intrinsic to the interior domain problem, and it can be recovered by the numerical scheme when choosing Γ sufficiently far from the obstacle (see Example 2).

To reformulate the above problem in operator form, following [1], we introduce the Hilbert space $V := H^1_{0,\Gamma_0}(\Omega) \times H_0^{-1/2}(\Gamma)$, equipped with the norm

$$\|\hat{u}\|_V^2 := \|u\|^2_{H^1(\Omega)} + \|\lambda\|^2_{H^{-1/2}(\Gamma)}, \quad \text{for } \hat{u} = (u, \lambda).$$

Then, we define the bilinear form $\mathcal{A} : V \times V \to \mathbf{R}$

$$\mathcal{A}(\hat{u}, \hat{v}) := a(u, v) - \langle \lambda, v \rangle_\Gamma + \langle \mu, u \rangle_\Gamma + 2\langle \mu, \mathrm{V}\lambda \rangle_\Gamma - 2\langle \mu, \mathrm{K}u \rangle_\Gamma,$$

for $\hat{u} = (u, \lambda)$ and $\hat{v} = (v, \mu)$, and the linear continuous operator $\mathcal{L}_f : V \to \mathbf{R}$

$$\mathcal{L}_f(\hat{v}) := (f, v)_{L^2(\Omega)}.$$

Hence, we rewrite Problem (8) as follows: find $\hat{u} \in V$ such that

$$\mathcal{A}(\hat{u}, \hat{v}) = \mathcal{L}_f(\hat{v}) \qquad \forall\, \hat{v} \in V, \tag{9}$$

whose well-posedness has been proved in [1] (see Lemma 2).
Finally, for the forthcoming analysis, it is convenient to rewrite $\mathcal{A} = \mathcal{B} + \mathcal{K}$ where the bilinear forms $\mathcal{B}, \mathcal{K} : V \times V \to \mathbf{R}$ are defined as follows:

$$\mathcal{B}(\hat{u}, \hat{v}) := a(u, v) - \langle \lambda, v \rangle_\Gamma + \langle \mu, u \rangle_\Gamma + 2\langle \mu, \mathrm{V}\lambda \rangle_\Gamma, \quad \mathcal{K}(\hat{u}, \hat{v}) := -2\langle \mu, \mathrm{K}u \rangle_\Gamma. \tag{10}$$

In the next sections, for the solution of Problem (9), we will describe a numerical approach consisting of a CVEM-BEM coupling. This method and the corresponding theoretical analysis is based on that proposed for the Helmholtz problem in [11], to which we refer whenever the theoretical results therein proved hold in our context as well. It is worth noting that

the theoretical analysis for the exterior Poisson problem cannot be obtained as a particular sub-case of the Helmholtz one given in [11], by simply choosing the wave number equal to zero. Indeed, the NRBC associated with the Laplace equation is different from that of the Helmholtz one, both for what concerns the kernel functions appearing in the boundary integral operators and the choice of the discrete function spaces for the approximation of the unknown λ. In fact, in this case, since we do not know a priori the asymptotic value α in (7c), the choice of the space $H_0^{-1/2}(\Gamma)$ becomes mandatory and, as a consequence, a proper discrete subspace of it is needed. Moreover, another important novelty of the theoretical study, with respect to that of [11], consists in the use of decoupled degrees of approximation for the interior CVEM and the BEM. This allows in particular the application of the CVEM with order higher than that of the BEM, a key aspect for the global scheme, the BEM requiring high efforts to efficiently compute the associated system matrices.

4 The Numerical Method

To describe the numerical approach we propose to solve (9), we start by introducing a suitable decomposition of the domain Ω, which consists of generic elements and is not limited to the more commonly used triangles or quadrilaterals.

Let us denote by E a generic "polygon" having at most one curved edge and by h_E its diameter; similarly, we denote by e a generic "edge", eventually curved, and by h_e its length. We introduce a sequence $\{\mathcal{T}_{h_\circ}\}_{h_\circ}$ of unstructured meshes $\mathcal{T}_{h_\circ} = \{E\}$, which cover the domain Ω, where $h_\circ := \max_{E\in\mathcal{T}_{h_\circ}} h_E$. We denote by $\mathcal{T}_{h_\partial}^\Gamma$ the decomposition of the artificial boundary Γ which, according to the regularity assumption required for Γ, consists of curvilinear parts. The subscript h_∂ denotes the mesh size defined by $h_\partial = \max_{e\in\mathcal{T}_{h_\partial}^\Gamma} h_e$.

We suppose there exists a constant $\varrho > 0$ such that for each $h_\circ$ and for each element $E \in \mathcal{T}_{h_\circ}$, E is star-shaped with respect to a ball of radius greater than ϱh_E and the length of any (eventually curved) edge of E is greater than ϱh_E.

For any $k \in \mathbf{N}$, let $P_k(E)$ be the space of polynomials of degree k defined on E, and $\Pi_k^{\nabla,E} : H^1(E) \to P_k(E)$ be the local polynomial H^1-projection, defined such that for $v \in H^1(E)$:

$$\begin{cases} \displaystyle\int_E \nabla\Pi_k^{\nabla,E} v \cdot \nabla q \,\mathrm{d}E = \int_E \nabla v \cdot \nabla q \,\mathrm{d}E \qquad \forall\, q \in P_k(E), \\ \displaystyle\int_{\partial E} \Pi_k^{\nabla,E} v \,\mathrm{d}s = \int_{\partial E} v \,\mathrm{d}s. \end{cases}$$

The local projector $\Pi_k^{\nabla,E}$ can be naturally extended to the global one $\Pi_k^\nabla : H^1(\Omega) \to P_k(\mathcal{T}_{h_\circ})$ as follows:

$$\left(\Pi_k^\nabla v\right)_{|_E} := \Pi_k^{\nabla,E} v_{|_E} \quad \forall\, v \in H^1(\Omega),$$

$P_k(\mathcal{T}_{h_\circ})$ being the space of piecewise polynomials with respect to the decomposition $\mathcal{T}_{h_\circ}$ of Ω. Moreover, let $\Pi_k^{0,E} : L^2(E) \to P_k(E)$ be the local polynomial L^2-projection operator, defined such that for $v \in L^2(E)$

$$\int_E \Pi_k^{0,E} v\, q \,\mathrm{d}E = \int_E v\, q \,\mathrm{d}E \qquad \forall\, q \in P_k(E).$$

By introducing the local bilinear form $a^{\mathrm{E}} : H^1(E) \times H^1(E) \to \mathbf{R}$ given by

$$a^{\mathrm{E}}(u, v) := \int_E \nabla u(\mathbf{x}) \cdot \nabla v(\mathbf{x}) \, \mathrm{d}\mathbf{x}, \tag{11}$$

we can write $a(u, v) = \sum_{E \in \mathcal{T}_{h_\circ}} a^{\mathrm{E}}(u, v)$.

Finally, we introduce the product space $H^1(\mathcal{T}_{h_\circ}) := \prod_{E \in \mathcal{T}_{h_\circ}} H^1(E)$ and define the associated broken H^1-norm:

$$\|v\|^2_{H^1(\mathcal{T}_{h_\circ})} := \sum_{E \in \mathcal{T}_{h_\circ}} \|v\|^2_{H^1(E)}.$$

To apply the Galerkin method to Problem (9), we introduce the discrete spaces $Q^{k_\circ}_{h_\circ} \subset H^1_{0,\Gamma_0}(\Omega)$ and $X^{k_\partial}_{h_\partial} \subset H_0^{-1/2}(\Gamma)$ associated with the meshes $\mathcal{T}_{h_\circ}$ and $\mathcal{T}^{\Gamma}_{h_\partial}$, respectively, and the product space $V^{\boldsymbol{k}}_{\boldsymbol{h}} := Q^{k_\circ}_{h_\circ} \times X^{k_\partial}_{h_\partial}$. Then, the Galerkin method consists in finding $\hat{u}_{\boldsymbol{h}} \in V^{\boldsymbol{k}}_{\boldsymbol{h}}$ such that

$$\mathcal{A}_{\boldsymbol{h}}(\hat{u}_{\boldsymbol{h}}, \hat{v}_{\boldsymbol{h}}) := \mathcal{B}_{\boldsymbol{h}}(\hat{u}_{\boldsymbol{h}}, \hat{v}_{\boldsymbol{h}}) + \mathcal{K}(\hat{u}_{\boldsymbol{h}}, \hat{v}_{\boldsymbol{h}}) = \mathcal{L}_{f,\boldsymbol{h}}(\hat{v}_{\boldsymbol{h}}) \quad \forall\, \hat{v}_{\boldsymbol{h}} \in V^{\boldsymbol{k}}_{\boldsymbol{h}}, \tag{12}$$

where $\mathcal{A}_{\boldsymbol{h}}, \mathcal{B}_{\boldsymbol{h}} : V^{\boldsymbol{k}}_{\boldsymbol{h}} \times V^{\boldsymbol{k}}_{\boldsymbol{h}} \to \mathbf{R}$ and $\mathcal{L}_{f,\boldsymbol{h}} : V^{\boldsymbol{k}}_{\boldsymbol{h}} \to \mathbf{R}$ are suitable approximations of $\mathcal{A}$, $\mathcal{B}$ and $\mathcal{L}_f$, respectively.

Proceeding analogously as in [11], we introduce sufficient conditions on the discrete spaces, on the bilinear form $\mathcal{B}_{\boldsymbol{h}}$ and on the linear operator $\mathcal{L}_{f,\boldsymbol{h}}$ to guarantee existence and uniqueness of the solution $\hat{u}_{\boldsymbol{h}} \in V^{\boldsymbol{k}}_{\boldsymbol{h}}$ and to prove convergence error estimates.

In particular we assume: for any $s \geq 1$

(H1.a) approximation in $Q^{k_\circ}_{h_\circ}$: for all $v \in H^{s+1}(\Omega)$

$$\inf_{v_{h_\circ} \in Q^{k_\circ}_{h_\circ}} \left\| v - v_{h_\circ} \right\|_{H^1(\Omega)} \lesssim h_\circ^{\min(s,k_\circ)} \|v\|_{H^{s+1}(\Omega)};$$

(H1.b) approximation in $X^{k_\partial}_{h_\partial}$: for all $\mu \in H^{s-1/2}(\Gamma) \cap H_0^{-1/2}(\Gamma)$

$$\inf_{\mu_{h_\partial} \in X^{k_\partial}_{h_\partial}} \left\| \mu - \mu_{h_\partial} \right\|_{H^{-1/2}(\Gamma)} \lesssim h_\partial^{\min(s,k_\partial)} \|\mu\|_{H^{s-1/2}(\Gamma)}.$$

In the above assumptions the notation $Q_1 \lesssim Q_2$ (as well as $Q_1 \gtrsim Q_2$ in what follows) means that the quantity Q_1 is bounded from above (resp. from below) by $c\, Q_2$, where c is a positive constant that, unless explicitly stated, does not depend on any relevant parameter involved in the definition of Q_1 and Q_2.

According to the definition of the $\|\cdot\|_V$ norm, (H1.a) and (H1.b) ensure the following approximation property for the product space $V^{\boldsymbol{k}}_{\boldsymbol{h}}$:

for $s \geq 1$, given $\hat{v} = (v, \mu) \in H^{s+1}(\Omega) \times (H^{s-1/2}(\Gamma) \cap H_0^{-1/2}(\Gamma))$, there exists $\hat{v}^I_{\boldsymbol{h}} = (v^I_{h_\circ}, \mu^I_{h_\partial}) \in V^{\boldsymbol{k}}_{\boldsymbol{h}}$ such that

$$\left\| \hat{v} - \hat{v}^I_{\boldsymbol{h}} \right\|_V \lesssim h_\circ^{\min(s,k_\circ)} \|v\|_{H^{s+1}(\Omega)} + h_\partial^{\min(s,k_\partial)} \|\mu\|_{H^{s-1/2}(\Gamma)}. \tag{13}$$

Recalling that the evaluation of the bilinear form $\mathcal{B}$ on elements of $V^{\boldsymbol{k}}_{\boldsymbol{h}}$ is well defined provided that $a(\cdot,\cdot)$ is split into the sum of the local contributions $a^{\mathrm{E}}(\cdot,\cdot)$, and assuming that the approximated bilinear form $\mathcal{B}_{\boldsymbol{h}}$ is well defined on the space $H^1(\mathcal{T}_{h_\circ})$, we further assume:

(H2.a) $k_\circ$-consistency: for all $\hat{q} \in P_{k_\circ}(\mathcal{T}_{h_\circ}) \times X_{h_\partial}^{k_\partial}$ and $\hat{v}_{\boldsymbol{h}} \in V_{\boldsymbol{h}}^{\boldsymbol{k}}$

$$\mathcal{B}_{\boldsymbol{h}}(\hat{q}, \hat{v}_{\boldsymbol{h}}) = \mathcal{B}(\hat{q}, \hat{v}_{\boldsymbol{h}}), \qquad \mathcal{B}_{\boldsymbol{h}}(\hat{v}_{\boldsymbol{h}}, \hat{q}) = \mathcal{B}(\hat{v}_{\boldsymbol{h}}, \hat{q});$$

(H2.b) continuity: for all $\hat{v}_{\boldsymbol{h}}, \hat{w}_{\boldsymbol{h}} \in V_{\boldsymbol{h}}^{\boldsymbol{k}}$

$$\left|\mathcal{B}_{\boldsymbol{h}}(\hat{v}_{\boldsymbol{h}}, \hat{w}_{\boldsymbol{h}})\right| \lesssim \left\|\hat{v}_{\boldsymbol{h}}\right\|_V \left\|\hat{w}_{\boldsymbol{h}}\right\|_V ;$$

(H2.c) ellipticity: for all $\hat{w}_{\boldsymbol{h}} \in V_{\boldsymbol{h}}^{\boldsymbol{k}}$

$$\mathcal{B}_{\boldsymbol{h}}(\hat{w}_{\boldsymbol{h}}, \hat{w}_{\boldsymbol{h}}) \gtrsim \left\|\hat{w}_{\boldsymbol{h}}\right\|_V^2 .$$

In the following theorem we show the validity of the inf-sup condition for the discrete bilinear form $\mathcal{A}_{\boldsymbol{h}}$.

Theorem 4.1 *Assuming* (H1.a), (H1.b) *and* (H2.a)–(H2.c), *for $h_\circ$ and h_∂ small enough, it holds that*

$$\sup_{\hat{v}_{\boldsymbol{h}} \in V_{\boldsymbol{h}}^{\boldsymbol{k}}, \hat{v}_{\boldsymbol{h}} \neq 0} \frac{\mathcal{A}_{\boldsymbol{h}}(\hat{w}_{\boldsymbol{h}}, \hat{v}_{\boldsymbol{h}})}{\left\|\hat{v}_{\boldsymbol{h}}\right\|_V} \gtrsim \left\|\hat{w}_{\boldsymbol{h}}\right\|_V \quad \forall\, \hat{w}_{\boldsymbol{h}} \in V_{\boldsymbol{h}}^{\boldsymbol{k}}.$$

Proof Following the proof of Lemma 4 in [1], it is possible to assert that, for any $\hat{w}_{\boldsymbol{h}} \in V_{\boldsymbol{h}}^{\boldsymbol{k}}$, there exists $\hat{v}_{\boldsymbol{h}} \in V_{\boldsymbol{h}}^{\boldsymbol{k}}$ such that

$$\left\|\hat{v}_{\boldsymbol{h}}\right\|_V \lesssim \left\|\hat{w}_{\boldsymbol{h}}\right\|_V \tag{14}$$

and

$$\mathcal{A}(\hat{w}_{\boldsymbol{h}}, \hat{v}_{\boldsymbol{h}}) \gtrsim (1 - h_\circ - h_\partial) \left\|\hat{w}_{\boldsymbol{h}}\right\|_V^2 . \tag{15}$$

By exploiting the decoupled assumptions (H1.a) and (H1.b) in Lemma 4.5 of [11], we obtain that for $\hat{v}_{\boldsymbol{h}} = (v_{h_\circ}, \mu_{h_\partial}) \in V_{\boldsymbol{h}}^{\boldsymbol{k}} \subset V$ there exists a unique $\hat{v}_{\boldsymbol{h}}^* = (v_{h_\circ}^*, \mu_{h_\partial}^*) \in V_{\boldsymbol{h}}^{\boldsymbol{k}}$ such that

$$\mathcal{B}_{\boldsymbol{h}}(\hat{w}_{\boldsymbol{h}}, \hat{v}_{\boldsymbol{h}}^*) = \mathcal{B}(\hat{w}_{\boldsymbol{h}}, \hat{v}_{\boldsymbol{h}}) \quad \forall\, \hat{w}_{\boldsymbol{h}} \in V_{\boldsymbol{h}}^{\boldsymbol{k}} \tag{16}$$

and

$$\left\|\mu_{h_\partial}^* - \mu_{h_\partial}\right\|_{H^{-3/2}(\Gamma)} \lesssim (h_\circ + h_\partial) \left\|\hat{v}_{\boldsymbol{h}}\right\|_V . \tag{17}$$

Recalling (10) and (12), and using (16), we get:

$$\begin{aligned}
\mathcal{A}_{\boldsymbol{h}}(\hat{w}_{\boldsymbol{h}}, \hat{v}_{\boldsymbol{h}}^*) &= \mathcal{B}_{\boldsymbol{h}}(\hat{w}_{\boldsymbol{h}}, \hat{v}_{\boldsymbol{h}}^*) + \mathcal{K}(\hat{w}_{\boldsymbol{h}}, \hat{v}_{\boldsymbol{h}}^*) = \mathcal{B}(\hat{w}_{\boldsymbol{h}}, \hat{v}_{\boldsymbol{h}}) + \mathcal{K}(\hat{w}_{\boldsymbol{h}}, \hat{v}_{\boldsymbol{h}}^*) \\
&= \mathcal{A}(\hat{w}_{\boldsymbol{h}}, \hat{v}_{\boldsymbol{h}}) + \mathcal{K}(\hat{w}_{\boldsymbol{h}}, \hat{v}_{\boldsymbol{h}}^*) - \mathcal{K}(\hat{w}_{\boldsymbol{h}}, \hat{v}_{\boldsymbol{h}}) \\
&= \mathcal{A}(\hat{w}_{\boldsymbol{h}}, \hat{v}_{\boldsymbol{h}}) - 2\langle \mu_{h_\partial}^* - \mu_{h_\partial}, \mathrm{K} w_{\boldsymbol{h}} \rangle_\Gamma .
\end{aligned}$$

By applying the Hölder's inequality and using (17) we have

$$\begin{aligned}
&\left|\langle \mu_{h_\partial}^* - \mu_{h_\partial}, \mathrm{K} w_{h_\circ} \rangle_{H^{-3/2}(\Gamma) \times H^{3/2}(\Gamma)}\right| \\
&\quad \lesssim \left\|\mu_{h_\partial}^* - \mu_{h_\partial}\right\|_{H^{-3/2}(\Gamma)} \left\|\mathrm{K} w_{h_\circ}\right\|_{H^{3/2}(\Gamma)} \\
&\quad \lesssim (h_\circ + h_\partial) \left\|\hat{v}_{\boldsymbol{h}}\right\|_V \left\|\mathrm{K} w_{h_\circ}\right\|_{H^{3/2}(\Gamma)} .
\end{aligned} \tag{18}$$

Then, using the continuity of $K : H^{1/2}(\Gamma) \to H^{3/2}(\Gamma)$ (see [1], formula (2.11)) and the trace theorem, we obtain

$$\left\|\mathrm{K} w_{h_\circ}\right\|_{H^{3/2}(\Gamma)} \lesssim \left\|w_{h_\circ}\right\|_{H^{1/2}(\Gamma)} \lesssim \left\|w_{h_\circ}\right\|_{H^1(\Omega)} \lesssim \left\|\hat{w}_{\boldsymbol{h}}\right\|_V ,$$

which, together with (18), implies

$$\left|\langle \mu_{h_\partial}^* - \mu_{h_\partial}, \mathrm{K} w_{h_\circ} \rangle_{H^{-3/2}(\Gamma) \times H^{3/2}(\Gamma)}\right| \lesssim (h_\circ + h_\partial) \left\|\hat{v}_{\boldsymbol{h}}\right\|_V \left\|\hat{w}_{\boldsymbol{h}}\right\|_V . \tag{19}$$

Finally, combining (15), (19) and (14), we get

$$\begin{aligned}\mathcal{A}_{\boldsymbol{h}}(\hat{w}_{\boldsymbol{h}}, \hat{v}^*_{\boldsymbol{h}}) &\gtrsim (1 - h_\circ - h_\partial) \left\|\hat{w}_{\boldsymbol{h}}\right\|_V^2 - (h_\circ + h_\partial) \left\|\hat{w}_{\boldsymbol{h}}\right\|_V \left\|\hat{v}_{\boldsymbol{h}}\right\|_V \\ &\gtrsim (1 - h_\circ - h_\partial) \left\|\hat{w}_{\boldsymbol{h}}\right\|_V^2,\end{aligned}$$

whence, for $h_\circ$ and h_∂ small enough, the claim follows. □

Theorem 4.1 allows us to prove the following convergence error estimate in the V-norm for Problem (12).

Theorem 4.2 *Assume there exist $k_\circ, k_\partial$ such that for all $s \geq 1$,* (H1.a),(H1.b)*, and* (H2.a)–(H2.c) *hold. Furthermore, assume that, for all $s \geq 1$, there exists $\sigma_s : L^2(\Omega) \to \mathbf{R}^+$ such that*

(H3.a) for all $\hat{v}_{\boldsymbol{h}} \in V_{\boldsymbol{h}}^{\boldsymbol{k}}$

$$\left|\mathcal{L}_f(\hat{v}_{\boldsymbol{h}}) - \mathcal{L}_{f,\boldsymbol{h}}(\hat{v}_{\boldsymbol{h}})\right| \lesssim \left(h_\circ^{min(s,k_\circ)} + h_\partial^{min(s,k_\partial)}\right) \left\|\hat{v}_{\boldsymbol{h}}\right\|_V \sigma_s(f).$$

Then, for $h_\circ$ and h_∂ small enough, Problem (12) *admits a unique solution $\hat{u}_{\boldsymbol{h}} \in V_{\boldsymbol{h}}^{\boldsymbol{k}}$ and if $\hat{u} = (u, \lambda)$, solution of Problem* (9)*, satisfies $\hat{u} \in H^{s+1}(\Omega) \times H^{s-1/2}(\Gamma)$, the following estimate holds*

$$\left\|\hat{u} - \hat{u}_{\boldsymbol{h}}\right\|_V \lesssim \left(h_\circ^{min(s,k_\circ)} + h_\partial^{min(s,k_\partial)}\right) \left(\|u\|_{H^{s+1}(\Omega)} + \sigma_s(f)\right).$$

Since the proof of Theorem 4.2 can be obtained by proceeding analogously as in Theorem 4.8 of [11], for brevity we omit it here.

In what follows we provide the error estimate in the weaker W-norm, where $W := L^2(\Omega) \times H^{-3/2}(\Gamma)$. To this aim, we start by assuming the following property:

(H3.b) consistency: for all $\hat{q} \in P_1(\mathcal{T}_{h_\circ}) \times X_{h_\partial}^{k_\partial}$

$$\mathcal{L}_{f,\boldsymbol{h}}(\hat{q}) = \mathcal{L}_f(\hat{q}).$$

Such assumption, together with some of those previously introduced, allows us to prove the following approximation error estimate for the operator $\mathcal{L}_f$.

Lemma 4.3 *Let $\hat{v} = (v, \mu) \in H^2(\Omega) \times H^{-1/2}(\Gamma)$, and let $v_{h_\circ}^I$ be the best approximation of v in $Q_{h_\circ}^{k_\circ}$. Under assumptions* (H1.a)*,* (H3.a) *and* (H3.b)*, for $s \geq 1$, it holds:*

$$\left|\mathcal{L}_f((v_{h_\circ}^I, \mu)) - \mathcal{L}_{f,\boldsymbol{h}}((v_{h_\circ}^I, \mu))\right| \lesssim h_\circ \left(h_\circ^{min(s,k_\circ)} + h_\partial^{min(s,k_\partial)}\right) \|v\|_{H^2(\Omega)} \sigma_s(f).$$

Proof Using (H3.b) and (H3.a), we can write

$$\begin{aligned}&|\mathcal{L}_f((v_{h_\circ}^I, \mu)) - \mathcal{L}_{f,\boldsymbol{h}}((v_{h_\circ}^I, \mu))| \\ &\quad= |\mathcal{L}_f((v_{h_\circ}^I, \mu)) - \mathcal{L}_{f,\boldsymbol{h}}((v_{h_\circ}^I, \mu)) - \mathcal{L}_f((\Pi_1^\nabla v, \mu)) + \mathcal{L}_{f,\boldsymbol{h}}((\Pi_1^\nabla v, \mu))| \\ &\quad= |\mathcal{L}_f((v_{h_\circ}^I - \Pi_1^\nabla v, 0)) - \mathcal{L}_{f,\boldsymbol{h}}((v_{h_\circ}^I - \Pi_1^\nabla v, 0))| \\ &\quad\lesssim \left(h_\circ^{\min(s,k_\circ)} + h_\partial^{\min(s,k_\partial)}\right) \|v_{h_\circ}^I - \Pi_1^\nabla v\|_{H^1(\mathcal{T}_{h_\circ})} \sigma_s(f).\end{aligned}$$

From (H1.a) and by using standard polynomial approximation estimates (see, for example, Lemma 4.3.8 in [25]), we get

$$\|\Pi_1^\nabla v - v_{h_\circ}^I\|_{H^1(\mathcal{T}_{h_\circ})} \leq \|\Pi_1^\nabla v - v\|_{H^1(\mathcal{T}_{h_\circ})} + \|v - v_{h_\circ}^I\|_{H^1(\Omega)} \lesssim h_\circ \|v\|_{H^2(\Omega)}, \tag{20}$$

which, combined with the previous estimate, leads to the claim. □

To prove the error estimate in the weaker W-norm, we introduce the dual space $W' := L^2(\Omega) \times H^{3/2}(\Gamma)$ and denote by $[\cdot,\cdot] : W \times W' \to \mathbf{R}$ the associated duality pairing. Further, we define the adjoint operator $\mathcal{A}^* : V \to V'$ as

$$\left(\mathcal{A}^*\hat{v}\right)(\hat{u}) := \mathcal{A}(\hat{u},\hat{v}),$$

which, by Lemma 3 in [1], is an isomorphism, whose inverse $\mathcal{A}^{*-1} : H^1(\Omega) \times H^{3/2}(\Gamma) \to H^2(\Omega) \times H^{1/2}(\Gamma)$ is continuous.

Theorem 4.4 *Assume that there exist $k_\circ$ and k_∂ and $\sigma_s : L^2(\Omega) \to \mathbf{R}^+$ such that, for all $s \geq 1$,* (H1.a),(H1.b), (H2.a)–(H2.c), (H3.a) *and* (H3.b) *hold. Then, for $h_\circ$ and h_∂ small enough, if $\hat{u}_{\boldsymbol{h}} \in V_{\boldsymbol{h}}^{\boldsymbol{k}}$ is the solution of Problem* (12) *and $\hat{u}$, solution of Problem* (9)*, satisfies $\hat{u} \in H^{s+1}(\Omega) \times H^{s-1/2}(\Gamma)$, for $s \geq 1$, the following estimate*

$$\left\|\hat{u} - \hat{u}_{\boldsymbol{h}}\right\|_W \lesssim (h_\circ + h_\partial)\left(h_\circ^{min(s,k_\circ)} + h_\partial^{min(s,k_\partial)}\right)\left(\|u\|_{H^{s+1}(\Omega)} + \sigma_s(f)\right)$$

holds.

Proof Let $\hat{w} \in W'$ and $\hat{v} := \mathcal{A}^{*-1}\hat{w}$ the unique element that, according to the above mentioned property of $\mathcal{A}^{*-1}$, satisfies $\hat{v} \in H^2(\Omega) \times H^{1/2}(\Gamma) \subset V$,

$$\mathcal{A}(\hat{z},\hat{v}) = \mathcal{A}(\mathcal{A}^{*-1}\hat{w},\hat{z}) = [\hat{z},\hat{w}] \quad \forall \hat{z} \in V \tag{21}$$

and $\left\|\hat{v}\right\|_{H^2(\Omega)\times H^{1/2}(\Gamma)} \lesssim \left\|\hat{w}\right\|_{W'}$.

Now, choosing $\hat{z} = \hat{u} - \hat{u}_{\boldsymbol{h}}$ in (21), where $\hat{u}$ and $\hat{u}_{\boldsymbol{h}}$ are the solutions of (9) and (12) respectively, and denoting by $\hat{v}_{\boldsymbol{h}}^I = (v_{h_\circ}^I, \mu_{h_\partial}^I) \in V_{\boldsymbol{h}}^{\boldsymbol{k}}$ the interpolant of $\hat{v}$, we obtain

$$\begin{aligned}
|\,[\hat{u} - \hat{u}_{\boldsymbol{h}}, \hat{w}]\,| &= \left|\mathcal{A}(\hat{u} - \hat{u}_{\boldsymbol{h}}, \hat{v})\right| \\
&= \left|\mathcal{A}(\hat{u} - \hat{u}_{\boldsymbol{h}}, \hat{v}) + \mathcal{A}_{\boldsymbol{h}}(\hat{u}_{\boldsymbol{h}}, \hat{v}_{\boldsymbol{h}}^I) - \mathcal{A}_{\boldsymbol{h}}(\hat{u}_{\boldsymbol{h}}, \hat{v}_{\boldsymbol{h}}^I) + \mathcal{A}(\hat{u} - \hat{u}_{\boldsymbol{h}}, \hat{v}_{\boldsymbol{h}}^I) - \mathcal{A}(\hat{u} - \hat{u}_{\boldsymbol{h}}, \hat{v}_{\boldsymbol{h}}^I)\right| \\
&\leq \left|\mathcal{A}(\hat{u} - \hat{u}_{\boldsymbol{h}}, \hat{v} - \hat{v}_{\boldsymbol{h}}^I)\right| + \left|\mathcal{L}_f(\hat{v}_{\boldsymbol{h}}^I) - \mathcal{L}_{f,\boldsymbol{h}}(\hat{v}_{\boldsymbol{h}}^I)\right| + \left|\mathcal{A}_{\boldsymbol{h}}(\hat{u}_{\boldsymbol{h}}, \hat{v}_{\boldsymbol{h}}^I) - \mathcal{A}(\hat{u}_{\boldsymbol{h}}, \hat{v}_{\boldsymbol{h}}^I)\right| \\
&\lesssim \left\|\hat{u} - \hat{u}_{\boldsymbol{h}}\right\|_V \left\|\hat{v} - \hat{v}_{\boldsymbol{h}}^I\right\|_V + h_\circ\left(h_\circ^{\min(s,k_\circ)} + h_\partial^{\min(s,k_\partial)}\right)\|v\|_{H^2(\Omega)}\,\sigma_s(f) \\
&\quad + \left|\mathcal{B}_{\boldsymbol{h}}(\hat{u}_{\boldsymbol{h}}, \hat{v}_{\boldsymbol{h}}^I) - \mathcal{B}(\hat{u}_{\boldsymbol{h}}, \hat{v}_{\boldsymbol{h}}^I)\right| =: I + II + III,
\end{aligned} \tag{22}$$

the last inequality following from the continuity of $\mathcal{A}$ and Lemma 4.3. By applying Theorem 4.2 and the interpolation property (13), we estimate

$$\begin{aligned}
I &\lesssim (h_\circ + h_\partial)\left(h_\circ^{\min(s,k_\circ)} + h_\partial^{\min(s,k_\partial)}\right)\left(\|u\|_{H^{s+1}(\Omega)} + \sigma_s(f)\right)\|\hat{v}\|_{H^2(\Omega)\times H^{1/2}(\Gamma)} \\
&\lesssim (h_\circ + h_\partial)\left(h_\circ^{\min(s,k_\circ)} + h_\partial^{\min(s,k_\partial)}\right)\left(\|u\|_{H^{s+1}(\Omega)} + \sigma_s(f)\right)\|\hat{w}\|_{W'},
\end{aligned} \tag{23}$$

and, since $\|v\|_{H^2(\Omega)} \leq \|\hat{v}\|_{H^2(\Omega)\times H^{1/2}(\Gamma)}$ we have

$$II \lesssim h_\circ\left(h_\circ^{\min(s,k_\circ)} + h_\partial^{\min(s,k_\partial)}\right)\|\hat{w}\|_{W'}\sigma_s(f). \tag{24}$$

To estimate III in (22), we add and subtract the terms $\mathcal{B}_{\boldsymbol{h}}((\Pi_{k_\circ}^\nabla u, \lambda), \hat{v}_{\boldsymbol{h}}^I)$ and $\mathcal{B}((\Pi_{k_\circ}^\nabla u, \lambda), \hat{v}_{\boldsymbol{h}}^I)$ which, for (H2.a), are equal. Hence we get

$$III = |\mathcal{B}_{\boldsymbol{h}}((u_{h_\circ} - \Pi_{k_\circ}^\nabla u, 0), \hat{v}_{\boldsymbol{h}}^I) - \mathcal{B}((u_{h_\circ} - \Pi_{k_\circ}^\nabla u, 0), \hat{v}_{\boldsymbol{h}}^I)|.$$

Similarly, adding and subtracting the two equal terms (see (H3.b))

$\mathcal{B}_{\boldsymbol{h}}((u_{h_\circ} - \Pi^\nabla_{k_\circ} u, 0), (\Pi^\nabla_{k_\circ} v, \mu^I_{h_\partial}))$ and $\mathcal{B}((u_{h_\circ} - \Pi^\nabla_{k_\circ} u, 0), (\Pi^\nabla_{k_\circ} v, \mu^I_{h_\partial}))$, we obtain

$$\begin{aligned} III \leq & |\mathcal{B}_{\boldsymbol{h}}((u_{h_\circ} - \Pi^\nabla_{k_\circ} u, 0), (v^I_{h_\circ} - \Pi^\nabla_1 v, 0))| \\ & + |\mathcal{B}((u_{h_\circ} - \Pi^\nabla_{k_\circ} u, 0), (v^I_{h_\circ} - \Pi^\nabla_1 v, 0))|. \end{aligned}$$

Using the continuity of $\mathcal{B}_{\boldsymbol{h}}$ (see (H2.b)) and of $\mathcal{B}$, we have

$$III \lesssim \left\| u_{h_\circ} - \Pi^\nabla_{k_\circ} u \right\|_{H^1(\mathcal{T}_{\boldsymbol{h}})} \left\| v^I_{h_\circ} - \Pi^\nabla_1 v \right\|_{H^1(\mathcal{T}_{\boldsymbol{h}})}.$$

The first factor of the above inequality is estimated, by using Theorem 4.2 and standard polynomial approximations, as follows

$$\begin{aligned} \|u_{h_\circ} - \Pi^\nabla_{k_\circ} u\|_{H^1(\mathcal{T}_{\boldsymbol{h}})} &\leq \|u_{h_\circ} - u\|_{H^1(\Omega)} + \left\| u - \Pi^\nabla_{k_\circ} u \right\|_{H^1(\mathcal{T}_{\boldsymbol{h}})} \\ &\lesssim \left(h_\circ^{\min(s,k_\circ)} + h_\partial^{\min(s,k_\partial)} \right) (\|u\|_{H^{s+1}(\Omega)} + \sigma_s(f)). \end{aligned}$$

Then, using (20), we obtain

$$\begin{aligned} III &\lesssim h_\circ \left(h_\circ^{\min(s,k_\circ)} + h_\partial^{\min(s,k_\partial)} \right) \left(\|u\|_{H^{s+1}(\Omega)} + \sigma_s(f) \right) \|v\|_{H^2(\Omega)} \\ &\lesssim h_\circ \left(h_\circ^{\min(s,k_\circ)} + h_\partial^{\min(s,k_\partial)} \right) \left(\|u\|_{H^{s+1}(\Omega)} + \sigma_s(f) \right) \|\hat{w}\|_{W'}. \end{aligned} \tag{25}$$

Finally, the assertion easily follows combining (22) with (23), (24) and (25). □

5 The CVEM-BEM Method

In this section we describe the discrete CVEM-BEM coupling procedure for the solution of Problem (9). In particular, we show that all the assumptions, introduced in Sect. 4 and used to prove Theorems 4.2 and 4.4, are satisfied. Referring to the notation introduced in Sect. 4, and denoting $P_{-1}(E) = \{0\}$, we consider for each $E \in \mathcal{T}_{h_\circ}$ the following local virtual space $Q^{k_\circ}_{h_\circ}(E)$ defined by

$$\begin{aligned} Q^{k_\circ}_{h_\circ}(E) := \big\{ & v_{h_\circ} \in H^1(E) : \Delta v_{h_\circ} \in P_{k_\circ - 2}(E), \\ & v_{h_\circ}|_{e_1} \in \widetilde{P}_{k_\circ}(e_1), v_{h_\circ}|_{e_i} \in P_{k_\circ}(e_i),\ i = 2, \ldots, n_{\mathrm{E}} \big\}, \end{aligned}$$

where $e_1, \ldots, e_{n_{\mathrm{E}}}$ denote the edges of the boundary of E, whose first element e_1 is assumed to be curved and parametrized by a local map $\gamma_E : I_E \to e_1$, and $\widetilde{P}_{k_\circ}(e_1) := \left\{ \widetilde{q} = q \circ \gamma_E^{-1} \ : \ q \in P_{k_\circ}(I_E) \right\}$.

We omit here, for brevity, the complete description of such space and we refer to [3, 12] for a deeper presentation. Further, since we will use some of the theoretical results proved in [11], we also refer to this latter, in particular for what concerns the notation.

On the basis of the definition of the local virtual space $Q^{k_\circ}_{h_\circ}(E)$, we construct the global virtual space

$$Q^{k_\circ}_{h_\circ} := \{ v_{h_\circ} \in H^1_{0,\Gamma_0} : v_{h_\circ|_E} \in Q^{k_\circ}_{h_\circ}(E),\ E \in \mathcal{T}_{h_\circ} \}.$$

The validity of Assumption (H1.a) is based on the proof of Lemma 5.2 in [11], in which the results hold both for the space $Q^{k_\circ}_{h_\circ}$ and for a suitable *enhanced* space associated with it. For

each $E \in \mathcal{T}_{h_\circ}$, in the spirit of the virtual element method, we define the approximation $a^{\mathrm{E}}_{h_\circ}$ of the bilinear form a^{E} (see definition (11)), as follows:

$$a^{\mathrm{E}}_{h_\circ}(u_{h_\circ}, v_{h_\circ}) := a^{\mathrm{E}}\left(\Pi^{\nabla,E}_{k_\circ} u_{h_\circ}, \Pi^{\nabla,E}_{k_\circ} v_{h_\circ}\right) + s^{\mathrm{E}}\left(\left(I - \Pi^{\nabla,E}_{k_\circ}\right) u_{h_\circ}, \left(I - \Pi^{\nabla,E}_{k_\circ}\right) v_{h_\circ}\right),$$

where s^E is the standard "*dofi-dofi*" stabilization term (see Eq. (3.22) of [26]).
The global approximate bilinear form $a_{h_\circ} : Q^{k_\circ}_{h_\circ} \times Q^{k_\circ}_{h_\circ} \to \mathbf{R}$ is then defined by summing up the local contributions

$$a_{h_\circ}(u_{h_\circ}, v_{h_\circ}) := \sum_{E \in \mathcal{T}_{\boldsymbol{h}}} a^{\mathrm{E}}_{h_\circ}(u_{h_\circ}, v_{h_\circ}).$$

The boundary element space $X^{k_\partial}_{h_\partial}$, associated with the artificial boundary Γ, is defined as follows:

$$X^{k_\partial}_{h_\partial} := \left\{\lambda \in L^2(\Gamma) \ : \lambda_{|_e} \in \widetilde{P}_{k_\partial - 1}(e), \ e \in \mathcal{T}^{\Gamma}_{h_\partial}\right\} \cap H_0^{-1/2}(\Gamma),$$

and we refer to [27] for the validity of the associated Assumption (H1.b). We then define the approximate bilinear form $\mathcal{B}_{\boldsymbol{h}} : V^{\boldsymbol{k}}_{\boldsymbol{h}} \times V^{\boldsymbol{k}}_{\boldsymbol{h}} \to \mathbf{R}$ as:

$$\mathcal{B}_{\boldsymbol{h}}(\hat{u}_{\boldsymbol{h}}, \hat{v}_{\boldsymbol{h}}) := a_{h_\circ}(u_{h_\circ}, v_{h_\circ}) - \langle \lambda_{h_\partial}, v_{h_\circ}\rangle_\Gamma + \langle \mu_{h_\partial}, u_{h_\circ}\rangle_\Gamma + 2\langle \mu_{h_\partial}, \mathrm{V}\lambda_{h_\partial}\rangle_\Gamma$$

for $\hat{u}_{\boldsymbol{h}} = (u_{h_\circ}, \lambda_{h_\partial})$, $\hat{v}_{\boldsymbol{h}} = (v_{h_\circ}, \mu_{h_\partial}) \in V^{\boldsymbol{k}}_{\boldsymbol{h}}$.

For these choices, from [11] (see Section 5.2), Assumptions (H2.a)-(H2.c) are satisfied. By approximating the linear operator $\mathcal{L}_f$ in a standard VEM way, in particular as in [28] (see Eq. (3.18)), and assuming $f \in H^{s-1}(\Omega)$, from Lemma 3.4 in [28], Assumption (H3.a) follows with $\sigma_s(f) = |f|_{H^{s-1}(\Omega)}$. Finally, Assumption (H3.b) is trivially satisfied.

6 Algebraic Details and Computational Issues

In this section we briefly describe the construction of the final linear system associated with the CVEM-BEM scheme, and we give some implementation details concerning the BEM matrices.

We start by re-ordering and splitting the complete index set $\mathcal{S}$ of the basis functions $\{\Phi_j\}_{j\in\mathcal{S}}$ of $Q^{k_\circ}_{h_\circ}$ as $\mathcal{S} = \mathcal{S}^I \cup \mathcal{S}^\Gamma$, where $\mathcal{S}^I$ and $\mathcal{S}^\Gamma$ denote the sets of indices related to the internal degrees of freedom and to those lying on Γ, respectively. Moreover, we denote by $\{\varphi_j\}_{j\in\mathcal{G}}$ the basis functions of $X^{k_\partial}_{h_\partial}$, $\mathcal{G}$ being the corresponding index set. In order to write the linear system associated with the discrete problem (12), we expand the unknown function $\hat{u}_{\boldsymbol{h}} = (u_{h_\circ}, \lambda_{h_\partial}) \in Q^{k_\circ}_{h_\circ} \times X^{k_\partial}_{h_\partial}$ as

$$\begin{aligned} u_{h_\circ}(\mathbf{x}) &:= \sum_{j\in\mathcal{S}} u^j_{h_\circ} \Phi_j(\mathbf{x}) \quad \text{with} \quad u^j_{h_\circ} = \mathrm{dof}_j(u_{h_\circ}), \\ \lambda_{h_\partial}(\mathbf{x}) &:= \sum_{j\in\mathcal{G}} \lambda^j_{h_\partial} \varphi_j(\mathbf{x}) \quad \text{with} \quad \lambda^j_{h_\partial} = \mathrm{dof}_j(\lambda_{h_\partial}). \end{aligned} \tag{26}$$

Hence, using the basis functions of $Q^{k_\circ}_{h_\circ}$ to test the discrete counterpart of equation (8a), we get for $i \in \mathcal{S}$

$$\sum_{j\in\mathcal{S}} u^j_{h_\circ} \sum_{E\in\mathcal{T}_{h_\circ}} a^{\mathrm{E}}_{h_\circ}(\Phi_j, \Phi_i) - \sum_{j\in\mathcal{G}} \lambda^j_{h_\partial} \langle \varphi_j, \Phi_i\rangle_\Gamma = \mathcal{L}_{f,\boldsymbol{h}}((\Phi_i, 0)). \tag{27}$$

To write the matrix form of the above linear system, we introduce the stiffness matrix $\mathbb{A}$ and the matrix $\mathbb{Q}$ whose entries are respectively defined by

$$\mathbb{A}_{ij} := \sum_{E\in\mathcal{T}_{h_\circ}} a^{\mathrm{E}}_{h_\circ}(\Phi_j,\Phi_i), \quad i,j\in\mathcal{S}, \qquad \mathbb{Q}_{ij} := \langle\varphi_j,\Phi_i\rangle_\Gamma, \quad i\in\mathcal{S}^\Gamma, j\in\mathcal{G}$$

and the column vectors $\mathbf{u} = \left[u^j_{h_\circ}\right]_{j\in\mathcal{S}}$, $\boldsymbol{\lambda} = \left[\lambda^j_{h_\partial}\right]_{j\in\mathcal{G}}$ and $\mathbf{f} = \left[\mathcal{L}_{f,\boldsymbol{h}}((\Phi_i,0))\right]_{i\in\mathcal{S}}$. In accordance with the splitting of the set of the degrees of freedom, we consider the block partitioned representation of the above matrices and vectors (with obvious meaning of the notation), and we rewrite equations (27) as follows:

$$\begin{bmatrix} \mathbb{A}^{II} & \mathbb{A}^{I\Gamma} \\ \mathbb{A}^{\Gamma I} & \mathbb{A}^{\Gamma\Gamma} \end{bmatrix} \begin{bmatrix} \mathbf{u}^I \\ \mathbf{u}^\Gamma \end{bmatrix} - \begin{bmatrix} \mathbf{0} \\ \mathbb{Q}\boldsymbol{\lambda} \end{bmatrix} = \begin{bmatrix} \mathbf{f}^I \\ \mathbf{f}^\Gamma \end{bmatrix}. \tag{28}$$

For what concerns the discretization of the BI-NRBC, by inserting (26) in (8b) and testing with the functions φ_i, $i\in\mathcal{G}$, we obtain

$$\begin{aligned} \sum_{j\in\mathcal{S}^\Gamma} u^j_{h_\circ} \left[\frac{1}{2}\int_\Gamma \Phi_j(\mathbf{x})\varphi_i(\mathbf{x})\mathrm{d}\Gamma_{\mathbf{x}} - \int_\Gamma \left(\int_\Gamma \frac{\partial G}{\partial \mathbf{n}_{\mathbf{y}}}(\mathbf{x},\mathbf{y})\Phi_j(\mathbf{y})\,\mathrm{d}\Gamma_{\mathbf{y}} \right) \varphi_i(\mathbf{x})\mathrm{d}\Gamma_{\mathbf{x}} \right] \\ + \sum_{j\in\mathcal{G}} \lambda^j_{h_\partial} \int_\Gamma \left(\int_\Gamma G(\mathbf{x},\mathbf{y})\varphi_j(\mathbf{y})\,\mathrm{d}\Gamma_{\mathbf{y}} \right) \varphi_i(\mathbf{x})\mathrm{d}\Gamma_{\mathbf{x}} = 0, \end{aligned} \tag{29}$$

that in matrix form reads

$$\left(\frac{1}{2}\mathbb{Q}^T - \mathbb{K}\right)\mathbf{u}^\Gamma + \mathbb{V}\boldsymbol{\lambda} = \mathbf{0}, \tag{30}$$

where

$$\mathbb{V}_{ij} := \int_\Gamma \left(\int_\Gamma G(\mathbf{x},\mathbf{y})\varphi_j(\mathbf{y})\mathrm{d}\Gamma_{\mathbf{y}} \right) \varphi_i(\mathbf{x})\mathrm{d}\Gamma_{\mathbf{x}},$$

$$\mathbb{K}_{ij} := \int_\Gamma \left(\int_\Gamma \frac{\partial G}{\partial \mathbf{n}_{\mathbf{y}}}(\mathbf{x},\mathbf{y})\Phi_j(\mathbf{y})\mathrm{d}\Gamma_{\mathbf{y}} \right) \varphi_i(\mathbf{x})\mathrm{d}\Gamma_{\mathbf{x}}.$$

By combining (28) with (30), we obtain the final linear system

$$\begin{bmatrix} \mathbb{A}^{II} & \mathbb{A}^{I\Gamma} & \mathbb{O} \\ \mathbb{A}^{\Gamma I} & \mathbb{A}^{\Gamma\Gamma} & -\mathbb{Q} \\ \mathbb{O} & \frac{1}{2}\mathbb{Q}^T - \mathbb{K} & \mathbb{V} \end{bmatrix} \begin{bmatrix} \mathbf{u}^I \\ \mathbf{u}^\Gamma \\ \boldsymbol{\lambda} \end{bmatrix} = \begin{bmatrix} \mathbf{f}^I \\ \mathbf{f}^\Gamma \\ \mathbf{0} \end{bmatrix}. \tag{31}$$

It is worth to point out that, since in the theoretical analysis we have assumed that the boundary integral operators are not approximated, it is crucial to compute the integrals defining the BEM entries of $\mathbb{V}$ and $\mathbb{K}$ with a high accuracy. Hence, to retrieve their approximation without affecting the overall accuracy of the coupled CVEM-BEM scheme, suitable efficient quadrature formulas must be considered. In [10] we have proposed and successfully applied a smoothing technique to weaken the log-singularity of the single layer operator V and to compute the corresponding entries with high accuracy by using the Gauss-Legendre product

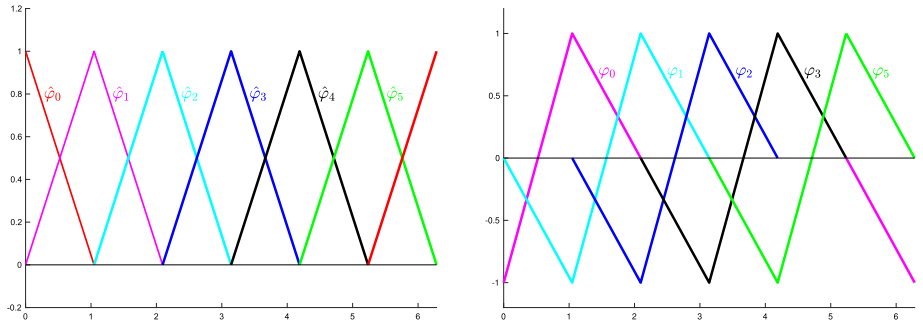

Fig. 2 Basis of $\hat{X}^2_{h_\partial}$ and $X^2_{h_\partial}$ in $[0, 2\pi)$

quadrature rule with few nodes. Such a strategy has been tuned for the standard nodal linear and quadratic basis functions and could, in principle, be adopted also in this context for the basis functions satisfying property (3). However, since the strategy associated with the standard Lagrangian basis is a well-established task, we take advantage of it by applying a computational trick. To describe this latter, we introduce the space

$$\widehat{X}^{k_\partial}_{h_\partial} := \{\lambda \in L^2(\Gamma) : \lambda_{|_e} \in \widetilde{P}_{k_\partial - 1}(e),\ e \in \mathcal{T}^\Gamma_{h_\partial}\} \subset H^{-1/2}(\Gamma),$$

whose Lagrangian basis functions are denoted by $\widehat{\varphi}_j$.

Further, we denote by $\widehat{\mathbb{V}}$, $\widehat{\mathbb{K}}$ and $\widehat{\mathbb{Q}}$ the matrices associated with the choice of the space $\widehat{X}^{k_\partial}_{h_\partial}$, which differ from $\mathbb{V}$, $\mathbb{K}$ and $\mathbb{Q}$ by the presence of the functions $\widehat{\varphi}_i$ instead of φ_i. In the forthcoming Remark 1 we detail the quadrature adopted to efficiently compute $\widehat{\mathbb{V}}$. Here we describe how to retrieve the matrices $\mathbb{V}$, $\mathbb{K}$ and $\mathbb{Q}$ from the corresponding $\widehat{\mathbb{V}}$, $\widehat{\mathbb{K}}$ and $\widehat{\mathbb{Q}}$. To this aim it is sufficient to define the functions φ_i as a suitable linear combination of the standard ones $\widehat{\varphi}_i$ and, hence, to combine accordingly the rows and/or the columns of $\widehat{\mathbb{V}}$, $\widehat{\mathbb{K}}$ and $\widehat{\mathbb{Q}}$. Such a combination depends on the order k_∂, on the shape of the artificial boundary Γ and on the associated mesh $\mathcal{T}^\Gamma_{h_\partial}$. In particular, for $k_\partial = 2$, we define $\varphi_i := c_i\widehat{\varphi}_i + \widehat{\varphi}_{i+1}$, where $\widehat{\varphi}_i$ and $\widehat{\varphi}_{i+1}$ are two consecutive piece-wise linear nodal basis functions. For $k_\partial = 3$, we distinguish the following two cases: a) $\varphi_{2i} := c_{2i}\widehat{\varphi}_{2i} + \widehat{\varphi}_{2i+1}$; b) $\varphi_{2i+1} := \widehat{\varphi}_{2i+1} + c_{2i+1}\widehat{\varphi}_{2i+2}$. The coefficients c_ℓ are chosen such that the relation $\int_\Gamma \varphi_\ell = 0$ is satisfied and are retrieved by applying a ν-point Gauss-Legendre quadrature formula, with ν chosen such that the integral over Γ of the associated $\widehat{\varphi}$ functions is accurately computed. It is worth noting that $\dim(X^{k_\partial}_{h_\partial}) = \dim(\widehat{X}^{k_\partial}_{h_\partial}) - 1$.

In Figs. 2 and 3, we show the basis functions of the spaces $\widehat{X}^{k_\partial}_{h_\partial}$ and $X^{k_\partial}_{h_\partial}$, with $k_\partial = 2, 3$ respectively, associated with the uniformly partitioned parametrization interval $[0, 2\pi)$ of the particular choice of a circle. For this choice, it is immediate to get $c_i = -1$ for $k_\partial = 2$, and $c_{2i} = c_{2i+1} = -2$ for $k_\partial = 3$.

Remark 1 We recall that the numerical integration difficulties in the computation of the $\widehat{\mathbb{V}}$ entries spring from the log-singularity of $G(r)$ near the origin, the latter being the kernel of the single layer operator V. To compute the corresponding integrals with high accuracy by few nodes, we have used the very simple and efficient polynomial smoothing technique proposed in [29], referred as the *q-smoothing* technique. It is worth noting that such technique is applied only when the distance r approaches zero. This case corresponds to the matrix entries belonging to the main diagonal and to the co-diagonals for which the supports of the basis functions overlap or are contiguous. After having introduced the *q-smoothing* transformation,

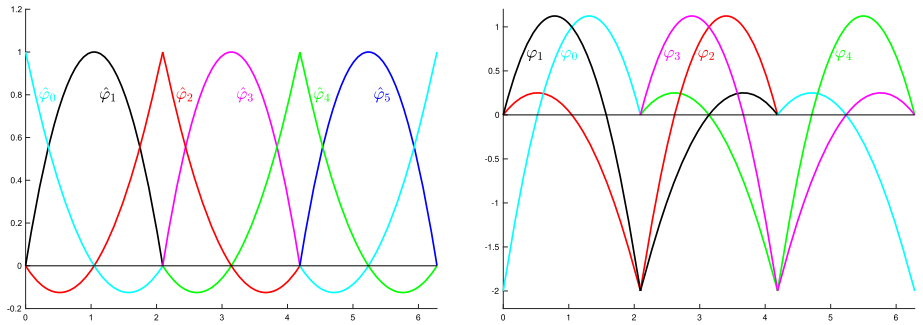

Fig. 3 Basis of $\hat{X}^3_{h_\partial}$ and $X^3_{h_\partial}$ in $[0, 2\pi)$

with $q = 3$, we have applied the n-point Gauss-Legendre quadrature rule with $n = 9$ for the outer integrals, and $n = 8$ for the inner ones (see [30] and Remark 3 in [10] for further details). For the computation of all the other integrals, we have applied a 9×8-point Gauss-Legendre product quadrature rule. Incidentally, we point out that the integrals involving the kernel function appearing in the double layer operator K, do not require a particular quadrature strategy, since its singularity $1/r$ is factored out by the same behaviour of the Jacobian near the origin. Hence, for the computation of the entries of the matrix $\widehat{\mathbb{K}}$, we have directly applied a 9×8-point Gauss-Legendre product quadrature rule.

The quadrature strategy described above guarantees the computation of all the mentioned integrals with a full precision accuracy (16-digit double precision arithmetic) for both $k_\partial = 2$ and $k_\partial = 3$.

7 Numerical Results

In this section, we present some numerical test to validate the theoretical results and to show the effectiveness of the proposed method.

For the generation of the partitioning $\mathcal{T}_{h_\circ}$ of the computational domain Ω, we have used, in the first two examples, the GMSH software to construct unstructured conforming meshes consisting of quadrilaterals (see [31]), while in the last two ones the Voronoi mesher PolyMesher (see [32]). If a polygon E has a (straight) edge bordering with the interior boundary or with the artificial one, we transform it into a curved boundary edge by means of a suitable parametrization. We remark that, even if in principle it is possible to fully decouple the interior and boundary meshes, we consider here for simplicity the boundary mesh inherited by the interior one, for which it turns out $h_\partial \leq h_\circ$. Furthermore, we point out that in all the numerical test we have considered $k_\partial = 2, 3$; larger values than those considered would require a tailored quadrature technique for the accurate computation of the BEM matrices that we have not performed yet. Since this usually is considered the bottleneck of the BEM, the use of decoupled approximation orders allows us to exploit the flexibility of the CVEM to retrieve high accuracy by increasing only the approximation order $k_\circ$. In Example 1 we will investigate this aspect.

Example 1 Let us consider the unbounded region Ω_e, external to the unit disk $\Omega_0 = \{\mathbf{x} = (x_1, x_2)^\top \in \mathbf{R}^2 \ : \ x_1^2 + x_2^2 \leq 1\}$. We consider Problem (1) with $f = 0$ and $g(\mathbf{x}) = x_1 + 2$ prescribed on the boundary $\Gamma_0 = \partial\Omega_0$. In this case, the exact solution $u(\mathbf{x})$ is known and its

Table 1 Example 1. Number of the degrees of freedom associated with the CVEM space

	lev. 0	lev. 1	lev. 2	lev. 3	lev. 4	lev. 5
$k_\circ = 2$	368	1, 376	5, 312	20, 864	82, 688	329, 216
$k_\circ = 3$	792	3, 024	11, 808	46, 656	185, 472	739, 584

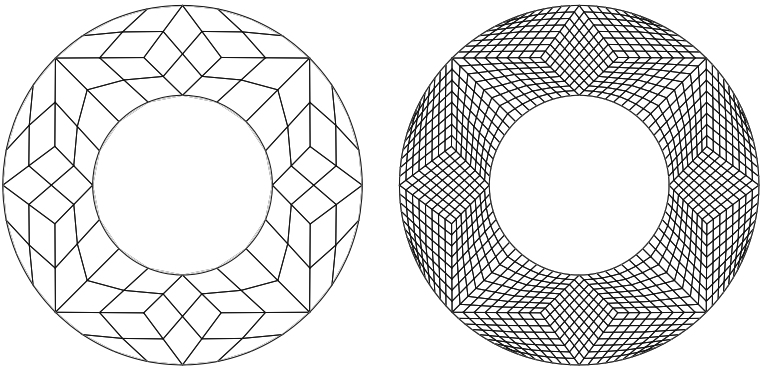

Fig. 4 Example 1. Meshes of Ω for lev. 0 (left plot) and lev. 2 (right plot)

expression is given by

$$u(\mathbf{x}) = \frac{x_1}{x_1^2 + x_2^2} + 2, \quad \mathbf{x} \in \Omega_e.$$

We choose as artificial boundary Γ the circle of radius 2, so that the finite computational domain Ω is the annulus bounded internally by Γ_0 and externally by Γ.

To develop a convergence analysis, we start by considering a coarse mesh, associated with the level of refinement zero (lev. 0), and all the successive refinements are obtained by halving each side of its elements. In Table 1, we report the total number of the degrees of freedom associated with the CVEM space, corresponding to each decomposition level of the computational domain, and the approximation orders $k_\circ = k_\partial = 2, 3$ (see Fig. 4 for the meshes corresponding to level 0 (left plot) and level 2 (right plot)).

To test our numerical approach and to validate the theoretical analysis, the order $k_\circ$ of the approximation spaces is chosen equal to 2 (quadratic) and 3 (cubic), and $k_\partial = k_\circ$. Moreover, recalling that the approximate solution $u_{h_\circ}$ is not known inside the polygons, as suggested in [12] we compute the H^1-seminorm and L^2-norm relative errors, and the corresponding EOC, by means of the following formulas:

- H^1-seminorm $\varepsilon_{\text{lev}}^{\nabla,k_\circ} := \sqrt{\dfrac{\sum_{E\in\mathcal{T}_{h_\circ}} \left|u-\Pi_{k_\circ}^{\nabla,E}u_{h_\circ}\right|^2_{H^1(E)}}{|u|^2_{H^1(\Omega)}}}$;
- L^2-norm $\varepsilon_{\text{lev}}^{0,k_\circ} := \sqrt{\dfrac{\sum_{E\in\mathcal{T}_{h_\circ}} \left\|u-\Pi_{k_\circ}^{0,E}u_{h_\circ}\right\|^2_{L^2(E)}}{\|u\|^2_{L^2(\Omega)}}}$;
- EOC $:= \log_2\left(\dfrac{\varepsilon_{\text{lev}+1}^{*,k_\circ}}{\varepsilon_{\text{lev}}^{*,k_\circ}}\right), \quad * \in \{\nabla, 0\}.$

Table 2 Example 1. Relative errors and EOC

lev.	$h_\circ$	L^2-norm				H^1-seminorm			
		$\varepsilon_{\text{lev}}^{0,2}$	EOC	$\varepsilon_{\text{lev}}^{0,3}$	EOC	$\varepsilon_{\text{lev}}^{\nabla,2}$	EOC	$\varepsilon_{\text{lev}}^{\nabla,3}$	EOC
0	$8.02e-01$	$4.26e-04$		$6.74e-05$		$4.96e-04$		$1.05e-04$	
			2.9		3.9		1.9		2.8
1	$4.28e-01$	$5.56e-05$		$4.58e-06$		$1.36e-04$		$1.51e-05$	
			3.0		4.0		2.0		3.0
2	$2.22e-01$	$7.05e-06$		$2.92e-07$		$3.46e-05$		$1.95e-06$	
			3.0		4.0		2.0		3.0
3	$1.13e-01$	$8.82e-07$		$1.84e-08$		$8.68e-06$		$2.45e-07$	
			3.0		4.0		2.0		3.0
4	$5.68e-02$	$1.10e-07$		$1.14e-09$		$2.17e-06$		$3.07e-08$	
			3.0		4.0		2.0		3.0
5	$2.85e-02$	$1.38e-08$		$7.35e-11$		$1.35e-07$		$3.93e-09$	

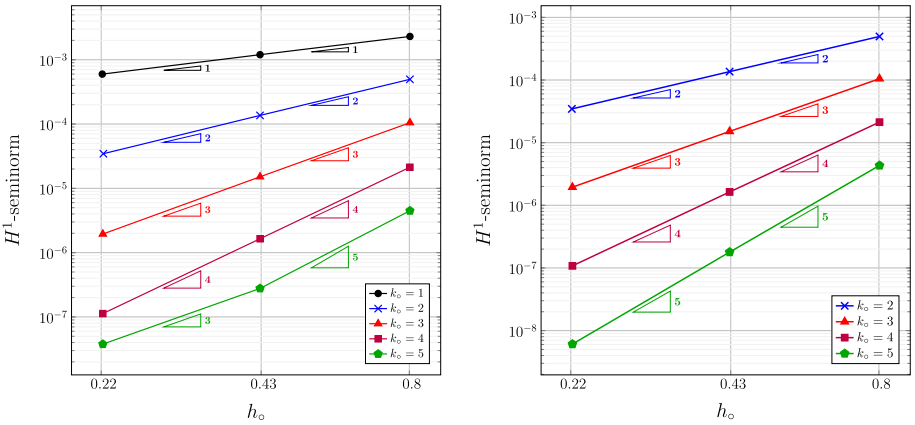

Fig. 5 Example 1. Behaviour of the H^1-seminorm relative error for $k_\partial = 2$ (left plot) and $k_\partial = 3$ (right plot) by varying $k_\circ$ and for lev. 0, 1, 2

In the above formulas the superscript $k_\circ = 2, 3$ refers to the approximation order of u, and the subscript lev refers to the refinement level. For what concerns the evaluation of these errors, to compute the associated integrals over polygons we have used the n-point quadrature formulas proposed in [33] and [34], which are exact for polynomials of degree at most $2n$. For curved polygons, we have applied the generalization of these formulas suggested in [12] (see Section 4.3). In both cases, we have chosen $n = 8$.

In Table 2 we report $\varepsilon_{\text{lev}}^{\nabla,k_\circ}$ and $\varepsilon_{\text{lev}}^{0,k_\circ}$ and the corresponding EOC by varying the refinement level from 0 to 5. As we can see the H^1-seminorm error and the L^2-norm error estimates confirm the expected convergence order of the method. For this example, we further investigate the possibility of choosing different approximation orders. In particular, since the meshes we have considered to generate Table 2 have the property $h_\circ = 2h_\partial$, we analyse the convergence of the scheme by fixing k_∂ and varying $k_\circ$. In Figs. 5 and 6 we report the behaviour of the H^1-seminorm and L^2-norm relative error, respectively. For each of them we fix in the left

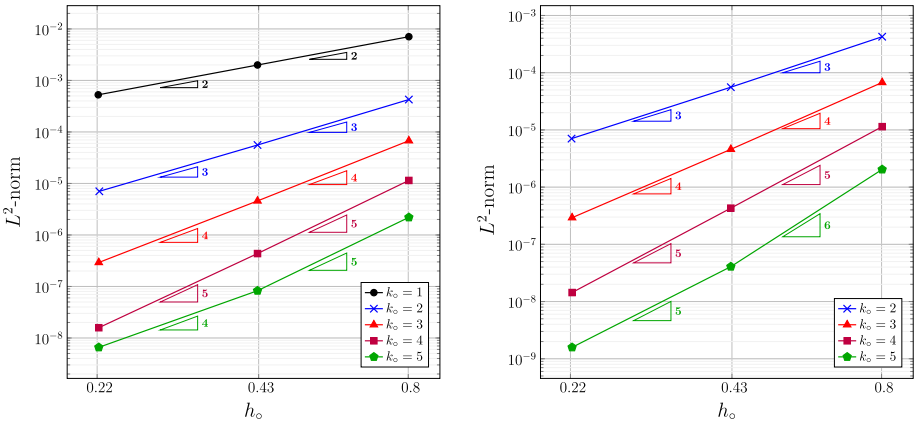

Fig. 6 Example 1. Behaviour of the L^2-norm relative error for $k_\partial = 2$ (left plot) and $k_\partial = 3$ (right plot) by varying $k_\circ$ and for lev. 0, 1, 2

plots $k_\partial = 2$ and in the right ones $k_\partial = 3$ and we report the errors associated with the refinement levels 0,1,2 by varying $k_\circ$. As we can see the CVEM convergence order dominates on the BEM one for each $k_\circ \leq 4$, while for larger values the BEM error is no longer negligible. Further, we observe that for $k_\partial = 3$ and $k_\circ = 5$ the CVEM H^1-convergence order is preserved, contrarily to that of the L^2 one. It is worth to point out that, for fixed values of $h_\circ$ and h_∂ and for fixed k_∂, the maximum value of $k_\circ$ such that the CVEM error is larger than that of the BEM is related to the dependence of the implicit constants of the error estimates on $k_\circ$ and k_∂. We are aware of a study on such dependency for some interior VEM problems (see for example [35, 36] and [37]), and this task, by no means trivial, is worth to be investigated. Finally, as we can see from Table 1, while the increasing behaviour of $k_\circ$ for a fixed mesh is approximately linear, that of lev. for a fixed $k_\circ$ is quadratic. Therefore, it is worth noting that it is more efficient, in terms of computational cost and memory saving, to use high order CVEM rather than to refine the mesh, the latter choice being also computationally demanding for what concerns the efficient computation of the BEM matrices.

Example 2 We consider the example proposed in [27] (and in [38]), for which Γ_0 is the boundary of the unit disk, centered at the origin of the cartesian axis, $f = 0$ and the datum g on Γ_0 is defined as

$$g(\mathbf{x}) = \begin{cases} x_1^4 & x_1 \geq 0, \\ 0 & x_1 < 0. \end{cases}$$

Solving the Dirichlet Laplace problem in polar coordinates, and expanding the solution in terms of the eigenvectors of the associated Sturm Liouville system, the solution in polar coordinates reads

$$u(\rho, \theta) = \frac{3}{16} + \frac{\rho^{-2}}{4}\cos(2\theta) + \frac{\rho^{-4}}{16}\cos(4\theta) + \frac{48}{\pi}\sum_{\substack{n=1 \\ n \text{ odd}}}^{\infty} \frac{(-1)^{(n-1)/2}\rho^{-n}}{n^5 - 20n^3 + 64n}\cos(n\theta),$$

from which we deduce that the asymptotic behaviour is given by the constant $\alpha = 3/16 = 0.1875$. We choose as artificial boundary the ellipse of semi-axes 50 and 15, so that the values of the numerical solution at the points $(-50, 0)$ and $(50, 0)$ can be considered good approximations of α. In Fig. 7 we compare the behaviour of the exact and numerical solutions in the

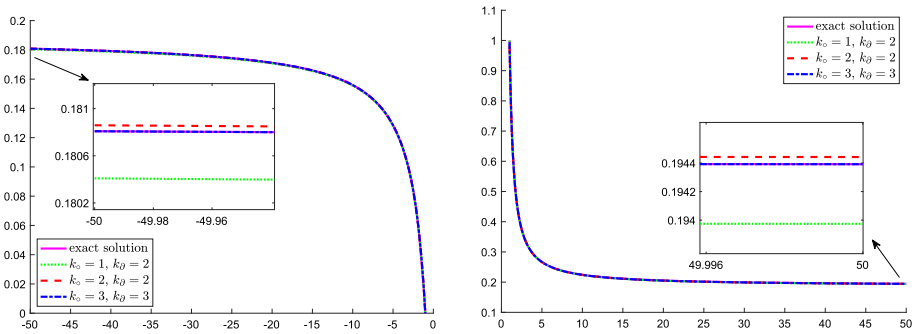

Fig. 7 Example 2. Exact and numerical solutions in $[-50, -1]$ (left plot) and $[1, 50]$ (right plot) by varying $k_\circ$ and k_∂

intervals $[-50, -1]$ (left plot) and $[1, 50]$ (right plot) for a fixed mesh of the computational domain and for different choices of the approximation orders. Besides noting a very good agreement of the approximate solutions, we have that the corresponding absolute errors at $(-50, 0)$ and $(50, 0)$ are approximately equal to $4.0e-04$ for $k_\circ = 1$ and $k_\partial = 2$, $5.0e-05$ for $k_\circ = k_\partial = 2$ and $1.0e-08$ for $k_\circ = k_\partial = 3$.

Example 3 In this example we consider an obstacle Ω_0 whose contour Γ_0 is only Lipschitz regular. In particular, $\Omega_0 = \Omega_0^1 \cup \Omega_0^2$, where Ω_0^1 and Ω_0^2 are the disks of radius 1.5 centred in $(-1, 0)$ and $(1, 0)$, respectively. We choose $f = 0$ and the Dirichlet datum

$$g(\mathbf{x}) := \begin{cases} -2x_1 + 2^{1/2}\left[\left(7x_1^2 + 2x_1 + \frac{1}{4}\right)^{1/2} + 2x_1^2 - 2x_1 - \frac{1}{2}\right]^{1/2} & x_1 \geq 0, \\ -2x_1 - 2^{1/2}\left[\left(7x_1^2 - 2x_1 + \frac{1}{4}\right)^{1/2} + 2x_1^2 + 2x_1 - \frac{1}{2}\right]^{1/2} & x_1 < 0, \end{cases}$$

for which the exact solution is given by (see [27])

$$u(\mathbf{x}) = -2x_1 + 2^{1/2}\mathrm{sgn}(x_1)\left[\left(\left(x_1^2 - x_2^2 + \frac{3}{4}\right)^2 + 4x_1^2x_2^2\right)^{1/2} + x_1^2 - x_2^2 + \frac{3}{4}\right]^{1/2}$$

(see Fig. 10, right plot). The artificial boundary Γ is the circle of radius 2.5. In Fig. 8 we show two meshes obtained by PolyMesher for the geometry Ω, corresponding to the refinements with 500 and 1500 elements, respectively. We point out that the meshes consist of elements with straight or curved edges, whose number varies from 4 to 8. The occurrences of the number of elements with respect to the number of edges are reported in Table 3, for the refinements consisting of a total number of 500, 1000, 1500, 2500 elements. By applying the CVEM-BEM coupling with the decoupled parameters $k_\partial = 2$ and $k_\circ = 1, 2, 3$ and using Voronoi meshes with 1000 and 1500 elements, we obtain the absolute errors reported in Fig. 9. As expected, the error is larger close to the cusps of the domain and decreases with the optimal rate as shown in Fig. 10.

Example 4 To complete the numerical examples, we apply our method to Problem (1) with a non null source f. The boundary Γ_0 is the ellipse with semi-axes 1.5 and 1, on which the Dirichlet condition $g = 0$ is prescribed, while Γ is a circle of radius 20. We choose the (computationally) compactly supported f such that the exact solution is (see Example 5 in [38])

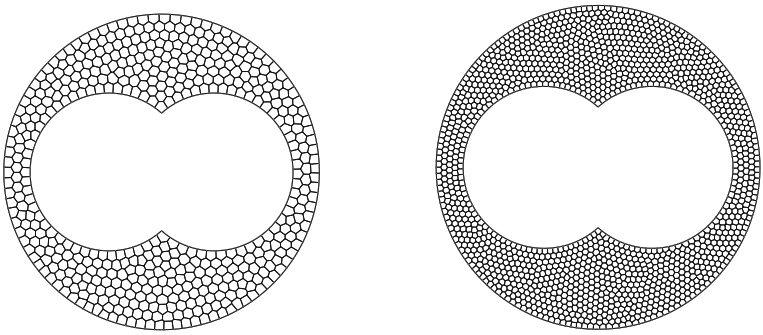

Fig. 8 Example 3. Voronoi meshes with 500 and 1500 elements

Table 3 Example 3. Number of the elements and the corresponding number of edges for some Voronoi meshes

Nr. of edges	Nr. of elements			
4	3	8	9	2
5	183	279	364	509
6	277	648	1035	1837
7	33	62	89	141
8	4	3	3	1
Total	500	1000	1500	2500

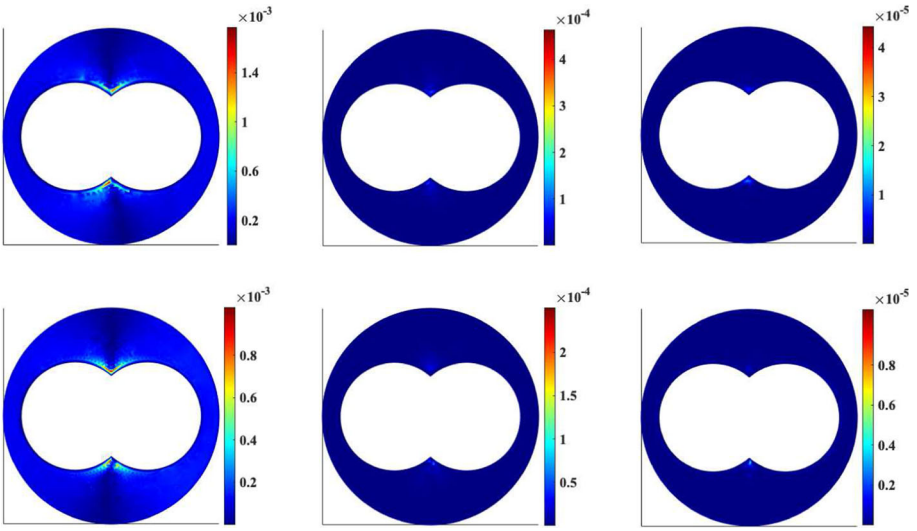

Fig. 9 Example 3. Absolute errors for refinements with 1000 (top row) and 1500 (bottom row) elements and for $k_\partial = 2$ and $k_\circ = 1, 2, 3$ (from left to right)

$$u(\mathbf{x}) = \frac{x_1^2 + 1.25x_2^2 - 1.25}{(x_1^2 + x_2^2 + 1)^2} e^{-0.1(x_1^2+x_2^2)}.$$

In Fig. 11, we show the behaviour of the approximate solution (left plot) and a zoom in a region surrounding the obstacle, where the corresponding absolute error is larger (right plot).

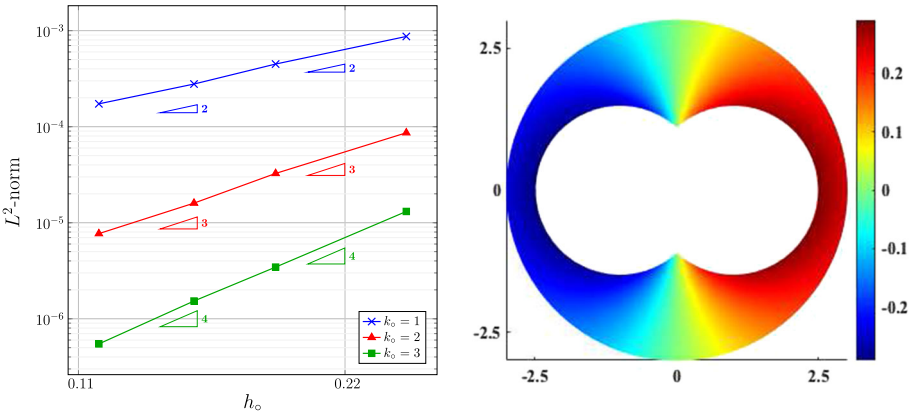

Fig. 10 Example 3. L^2-norm convergence rate for $k_\partial = 2$, $k_\circ = 1, 2, 3$ and the Voronoi meshes with 500, 1000, 1500, 2500 elements (left plot) and the exact solution (right plot)

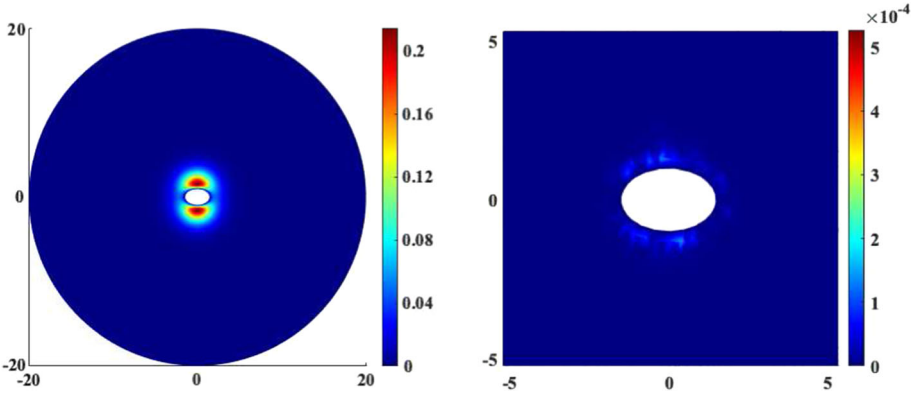

Fig. 11 Example 4. Behaviour of the approximate solution (left plot) and a zoom of the corresponding absolute error in $[-5, 5] \times [-5, 5]$ (right plot) for a refinement with 10000 elements, for $k_\partial = 2$ and $k_\circ = 3$

We point out that this last aspect is in agreement with the analogous presented in [38], where a mortar approach has been employed with non matching meshes on the BEM-FEM interface. Here, we use decoupled orders $k_\partial = 2$ and $k_\circ = 3$ on a Voronoi mesh with 10000 elements.

8 Conclusions

We have proposed and analysed the coupling of a CVEM with the one-equation BEM to solve 2D exterior Poisson problems. The peculiarity of the scheme consists in the use of decoupled approximation orders for the interior CVEM and for the BI-NRBC. This strategy has allowed us to exploit the well-known flexibility of the CVEM to retrieve an accurate solution by a low order approximation for the BEM. Since high order BEMs require non-trivial computational efforts to efficiently evaluate the matrix entries of the associated integral operators, the advantage of using a low order BEM turns out to be a key aspect to achieve a good accuracy and convergence rate weighted against computational costs.

The good performances obtained by applying the proposed scheme to elliptic problems, encourage us to consider it within other contexts, such as time dependent exterior problems

for which both the pure BEM and its coupling with standard interior domain methods could become prohibitive.

Acknowledgements The authors are grateful to the referees for their careful reading of the manuscript and their useful comments. This work was performed as part of the GNCS-INdAM 2020 research program *"Metodologie innovative per problemi di propagazione di onde in domini illimitati: aspetti teorici e computazionali"*. The third author was partially supported by MIUR grant *"Dipartimenti di Eccellenza 2018-2022"*, CUP E11G18000350001.

Funding Open access funding provided by Politecnico di Torino within the CRUI-CARE Agreement.

Data Availability Enquiries about data availability should be directed to the authors.

Declarations

Competing interests The authors have not disclosed any competing interests.

References

1. Johnson, C., Nédélec, J.-C.: On the coupling of boundary integral and finite element methods. Math. Comp. **35**(152), 1063–1079 (1980). https://doi.org/10.2307/2006375
2. Sauter, S.A., Schwab, C.: Boundary Element Methods. Springer Series in Computational Mathematics, vol. 39. https://doi.org/10.1007/978-3-540-68093-2
3. Beirão da Veiga, L., Brezzi, F., Cangiani, A., Manzini, G., Marini, L.D., Russo, A.: Basic principles of virtual element methods. Math. Models Methods Appl. Sci. **23**(1), 199–214 (2013). https://doi.org/10.1142/S0218202512500492
4. Antonietti, P.F., Manzini, G., Verani, M.: The conforming virtual element method for polyharmonic problems. Comput. Math. Appl. **79**(7), 2021–2034 (2020). https://doi.org/10.1016/j.camwa.2019.09.022
5. Mascotto, L., Perugia, I., Pichler, A.: A nonconforming Trefftz virtual element method for the Helmholtz problem. Math. Models Methods Appl. Sci. **29**(9), 1619–1656 (2019). https://doi.org/10.1142/S0218202519500301
6. Artioli, E., Marfia, S., Sacco, E.: VEM-based tracking algorithm for cohesive/frictional 2D fracture. Comput. Methods Appl. Mech. Engrg. **365**, 112956–21 (2020). https://doi.org/10.1016/j.cma.2020.112956
7. Beirão da Veiga, L., Canuto, C., Nochetto, R.H., Vacca, G.: Equilibrium analysis of an immersed rigid leaflet by the virtual element method. Math. Models Methods Appl. Sci. **31**(7), 1323–1372 (2021). https://doi.org/10.1142/S0218202521500275
8. Gatica, G.N., Meddahi, S.: On the coupling of VEM and BEM in two and three dimensions. SIAM J. Numer. Anal. **57**(6), 2493–2518 (2019). https://doi.org/10.1137/18M1202487
9. Gatica, G.N., Meddahi, S.: Coupling of virtual element and boundary element methods for the solution of acoustic scattering problems. J. Numer. Math. **28**(4), 223–245 (2020). https://doi.org/10.1515/jnma-2019-0068
10. Desiderio, L., Falletta, S., Scuderi, L.: A Virtual Element Method coupled with a Boundary Integral Non Reflecting condition for 2D exterior Helmholtz problems. Comput. Math. Appl. **84**, 296–313 (2021). https://doi.org/10.1016/j.camwa.2021.01.002
11. Desiderio, L., Falletta, S., Ferrari, M., Scuderi, L.: On the coupling of the curved virtual element method and the one-equation boundary element method for 2d exterior Helmholtz problems. SIAM J. Numer. Anal. to appear

12. Beirão da Veiga, L., Russo, A., Vacca, G.: The virtual element method with curved edges. ESAIM Math. Model. Numer. Anal. **53**(2), 375–404 (2019). https://doi.org/10.1051/m2an/2018052
13. Beirão da Veiga, L., Brezzi, F., Marini, L.D., Russo, A.: Polynomial preserving virtual elements with curved edges. Math. Models Methods Appl. Sci. **30**(8), 1555–1590 (2020). https://doi.org/10.1142/S0218202520500311
14. Rjasanow, S., Weißer, S.: Higher order BEM-based FEM on polygonal meshes. SIAM J. Numer. Anal. **50**(5), 2357–2378 (2012). https://doi.org/10.1137/110849481
15. Anand, A., Ovall, J.S., Weißer, S.: A Nyström-based finite element method on polygonal elements. Comput. Math. Appl. **75**(11), 3971–3986 (2018). https://doi.org/10.1016/j.camwa.2018.03.007
16. Anand, A., Ovall, J.S., Reynolds, S.E., Weißer, S.: Trefftz finite elements on curvilinear polygons. SIAM J. Sci. Comput. **42**(2), 1289–1316 (2020). https://doi.org/10.1137/19M1294046
17. Sevilla, R., Fernández-Méndez, S., Huerta, A.: Comparison of high-order curved finite elements. Internat. J. Numer. Methods Engrg. **87**(8), 719–734 (2011). https://doi.org/10.1002/nme.3129
18. Botti, L., Di Pietro, D.A.: Assessment of hybrid high-order methods on curved meshes and comparison with discontinuous Galerkin methods. J. Comput. Phys. **370**, 58–84 (2018). https://doi.org/10.1016/j.jcp.2018.05.017
19. Brezzi, F., Lipnikov, K., Shashkov, M.: Convergence of mimetic finite difference method for diffusion problems on polyhedral meshes with curved faces. Math. Models Methods Appl. Sci. **16**(2), 275–297 (2006). https://doi.org/10.1142/S0218202506001157
20. Burman, E., Cicuttin, M., Delay, G., Ern, A.: An unfitted hybrid high-order method with cell agglomeration for elliptic interface problems. SIAM J. Sci. Comput. **43**(2), 859–882 (2021). https://doi.org/10.1137/19M1285901
21. Brezzi, F., Johnson, C.: On the coupling of boundary integral and finite element methods. Calcolo **16**(2), 189–201 (1979). https://doi.org/10.1007/BF02575926
22. Costabel, M.: Symmetric Methods for the Coupling of Finite Elements and Boundary Elements (invited Contribution), 411–420. Comput. Mech., Southampton (1987). https://doi.org/10.1007/978-3-662-21908-9_26
23. Han, H.D.: A new class of variational formulations for the coupling of finite and boundary element methods. J. Comput. Math. **8**(3), 223–232 (1990)
24. Hsiao, G.C., Wendland, W.L.: Boundary Integral Equations. Applied Mathematical Sciences, vol. 164, 618. Springer, Berlin (2008). https://doi.org/10.1007/978-3-540-68545-6
25. Brenner, S.C., Scott, L.R.: The Mathematical Theory of Finite Element Methods, 3rd edn. Texts in Applied Mathematics, vol. 15, 397. Springer, New York (2008). https://doi.org/10.1007/978-0-387-75934-0
26. Beirão da Veiga, L., Brezzi, F., Marini, L.D., Russo, A.: The hitchhiker's guide to the virtual element method. Math. Models Methods Appl. Sci. **24**(8), 1541–1573 (2014). https://doi.org/10.1142/S021820251440003X
27. Le Roux, M.N.: Méthode d'éléments finis pour la résolution numérique de problèmes extérieurs en dimension 2. RAIRO Anal. Numér. **11**(1), 27–60112 (1977). https://doi.org/10.1051/m2an/1977110100271
28. Brenner, S.C., Guan, Q., Sung, L.Y.: Some estimates for virtual element methods. Comput. Methods Appl. Math. **17**(4), 553–574 (2017). https://doi.org/10.1515/cmam-2017-0008
29. Monegato, G., Scuderi, L.: Numerical integration of functions with boundary singularities. J. Comput. Appl. Math. **112**(1–2), 201–214 (1999). https://doi.org/10.1016/S0377-0427(99)00230-7
30. Falletta, S., Monegato, G., Scuderi, L.: A space-time BIE method for wave equation problems: the (two-dimensional) Neumann case. IMA J. Numer. Anal. **34**(1), 390–434 (2014). https://doi.org/10.1093/imanum/drs040
31. Geuzaine, C., Remacle, J.F.: Gmsh: a three-dimensional finite element mesh generator with built-in pre- and post processing facilities. Internat. J. Numer. Methods Engrg. **79**, 1309–1331 (2009). https://doi.org/10.1002/nme.2579
32. Talischi, C., Paulino, G.H., Pereira, A., Menezes, I.F.M.: PolyMesher: a general-purpose mesh generator for polygonal elements written in Matlab. Struct. Multidiscip. Optim. **45**(3), 309–328 (2012). https://doi.org/10.1007/s00158-011-0706-z
33. Sommariva, A., Vianello, M.: Product Gauss cubature over polygons based on Green's integration formula. BIT **47**(2), 441–453 (2007). https://doi.org/10.1007/s10543-007-0131-2
34. Sommariva, A., Vianello, M.: Gauss-Green cubature and moment computation over arbitrary geometries. J. Comput. Appl. Math. **231**(2), 886–896 (2009). https://doi.org/10.1016/j.cam.2009.05.014
35. Beirão da Veiga, L., Chernov, A., Mascotto, L., Russo, A.: Basic principles of *hp* virtual elements on quasiuniform meshes. Math. Models Methods Appl. Sci. **26**(8), 1567–1598 (2016). https://doi.org/10.1142/S021820251650038X

36. Beirão da Veiga, L., Chernov, A., Mascotto, L., Russo, A.: Exponential convergence of the hp virtual element method in presence of corner singularities. Numer. Math. **138**(3), 581–613 (2018). https://doi.org/10.1007/s00211-017-0921-7
37. Beirão da Veiga, L., Manzini, G., Mascotto, L.: A posteriori error estimation and adaptivity in hp virtual elements. Numer. Math. **143**(1), 139–175 (2019). https://doi.org/10.1007/s00211-019-01054-6
38. Bertoluzza, S., Falletta, S.: FEM solution of exterior elliptic problems with weakly enforced integral non reflecting boundary conditions. J. Sci. Comput. **81**(2), 1019–1049 (2019). https://doi.org/10.1007/s10915-019-01048-4